THE JOURNAL OF PHYSICAL CHEMISTRY C
A JOURNAL OF THE AMERICAN CHEMICAL SOCIETY

pubs.acs.org/JPCC

Article

Advanced Spectroscopic and Computational Studies of a Cobalt(II) Coordination Polymer with Single-Ion-Magnet Properties

Pagnareach Tin, Alexandria N. Bone, Nhat N. Bui, Yi-Quan Zhang, Tieyan Chang, Duncan H. Moseley, Mykhaylo Ozerov, J. Krzystek, Yongqiang Cheng, Luke L. Daemen, Xiaoping Wang, Likai Song, Yu-Sheng Chen, Dong Shao, Xin-Yi Wang, Xue-Tai Chen, and Zi-Ling Xue*

Cite This: *J. Phys. Chem. C* 2022, 126, 13268−13283

Read Online

ACCESS | Metrics & More | Article Recommendations | Supporting Information

ABSTRACT: Two-dimensional (2D) coordination polymer (CP) $[Co^{III}(CN)_6]_2[Co^{II}(TODA)]_3{\cdot}7H_2O$ (TODA = 1,4,10-trioxa-7,13-diazacyclopentadecane, **Co-TODA**) was reported earlier to show field-induced slow magnetic relaxation, displaying single-ion magnet (SIM) behaviors. Most SIMs are molecular compounds with fewer adopting coordination polymer (CP) or metal−organic framework (MOF) structures. In the current work, magnetic and phonon properties of **Co-TODA** have been studied by advanced spectroscopies and computations. The combined use of far-IR magneto-spectroscopy (FIRMS) and variable-temperature (VT) high-frequency and -field electron paramagnetic resonance (HFEPR) gives spin Hamiltonian (SH) parameters: Axial zero-field splitting (ZFS) parameter D as $+38.0(1.0) \leq D \ll +40.2(1.0)$ cm^{-1} and rhombic ZFS parameter E as $0 \ll |E| \leq 7.3(1.0)$ cm^{-1}, showing that **Co-TODA** has the easy-plane magnetic anisotropy. Two Co^{II} centers in the CP, as determined by synchrotron single-crystal X-ray diffraction at 15(2) K, show similar magnetic properties indistinguishable in FIRMS at 5.3(3) K or in HFEPR at 5−150 K. Ab initio calculations explore the origin of the magnetic anisotropy and magnetostructural correlations. VT inelastic neutron scattering (INS) spectra of **Co-TODA** have been obtained to show the phonon properties of the CP. Density functional theory (DFT) calculations, giving both a calculated INS spectrum and spin distributions in **Co-TODA**, demonstrate that, compared with other high-spin Co^{II} complexes, the larger the spin density on a metal ion, the larger the ZFS in the complex. Pulsed X-band EPR studies probe relaxations of the Co^{II} ions from the $M_S = +1/2$ to $-1/2$ state in the ground Kramers doublet (KD), yielding spin−lattice (T_1) and spin−spin relaxation (T_2) times. The work reported here highlights the versatility and power of the spectroscopic techniques and computations in the characterization of magnetic and phonon properties of a CP and the understanding of its magnetic anisotropy.

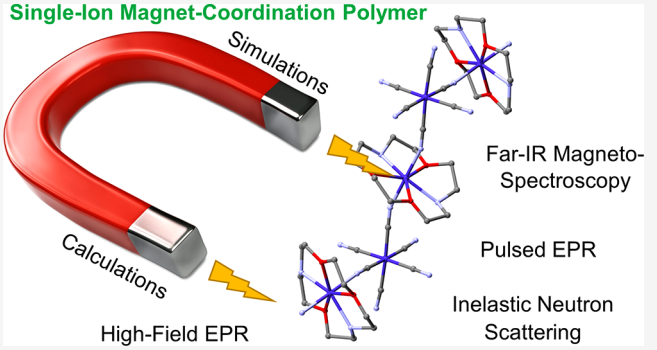

INTRODUCTION

Single-molecule magnets (SMMs) exhibit slow relaxation of their magnetization, a desired property in retaining the information stored,[1−17] with potential applications in, e.g., molecular spintronics and high-density information storage. One current focus of the SMM research is mononuclear complexes containing one metal ion (SIMs). Reported SIMs are mostly molecular compounds. There are fewer SIMs as coordination polymers (CPs) or metal−organic frameworks (MOFs) which provide the necessary structures for scaling the magnets to the macroscopic level,[18] although MOFs and CPs,[19−21] including cyanometallate CPs,[19,20] are of intense current interest with many applications. SIMs with CP structures can be achieved using long organic spacers to separate the metal nodes and lower their interactions in space.

When the first-order angular momentum is quenched in $S = 3/2$ (high-spin) Co^{II} compounds, second-order spin−orbit coupling (SOC) may lead to the separation of the ground electronic state at zero magnetic field [known as zero-field splitting (ZFS)].[8,22−24] The axial ZFS parameter D represents the anisotropy in the z-direction (from the x,y-directions). The rhombic E parameter shows the anisotropy between the x- and y-direction. A SMM displays magnetic hysteresis below the blocking temperature (T_B) as well as an energy barrier to spin reversal from $+M_S$ to $-M_S$.[25,26] In other words, relaxation of the SMM depends on the energy barrier for the spin reversal, which in turn depends on the ZFS parameters D and E.[7,27]

The ZFS diagram for $D > 0$, $S = 3/2$ complexes is given in Figure 1,[28,29] showing that the crystal field anisotropy split the

Received: May 4, 2022
Revised: July 6, 2022
Published: July 28, 2022

https://doi.org/10.1021/acs.jpcc.2c03083
J. Phys. Chem. C 2022, 126, 13268−13283

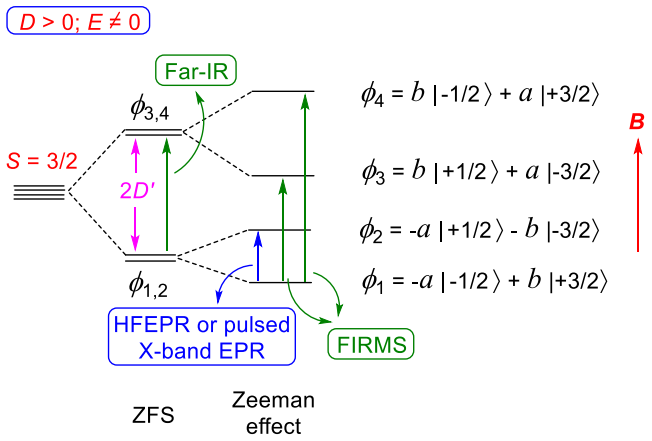

Figure 1. Energy splitting diagram for $S = 3/2$ complexes when $D > 0$, where $D' = (D^2 + 3E^2)^{1/2}$. $M_S = \pm 1/2$ and $\pm 3/2$ are nominal labels for the levels due to the mixing of the two spin states when $E \neq 0$.[28] Mixing coefficients $a = \cos\beta$ and $b = \sin\beta$ are described by the mixing angle β obtained from the spin Hamiltonian (SH) ($S = 3/2$).[32,33] Mixing is a function of the rhombicity, since $\tan 2\beta = \sqrt{3}\,(E/D)$. In the absence of the external magnetic field $\boldsymbol{B}$, the excitation from $M_S = \pm 1/2$ to $\pm 3/2$ KD may be observed in far-IR spectroscopy. For **Co-TODA** at 5 K inside the magnetic field $\boldsymbol{B}$, Co^{II} centers are mostly at the ground ϕ_1 state. As a result of mixing, the excitation $\phi_1 \rightarrow \phi_4$ is also spin-allowed (from the $M_S = -1/2$ component in both wavefunctions). Thus, the two inter-Kramers excitations $\phi_1 \rightarrow \phi_3$ and $\phi_1 \rightarrow \phi_4$ are the expected transitions and can be observed by far-IR magneto-spectroscopy (FIRMS) for large ZFS splitting. In the current studies, intra-Kramers transition $\phi_1 \rightarrow \phi_2$ inside the magnetic field $\boldsymbol{B}$ was probed by high-field electron paramagnetic resonance (HFEPR) and pulsed EPR, although the two spectroscopies were operated at significantly different magnetic fields and spectral frequencies.

four $(2S + 1)$ degenerate states into $M_S = \pm 1/2$ and $\pm 3/2$ Kramers doublets (KDs). When the crystallographic point group symmetry of the metal site (paramagnetic center) is axial and 3-fold or higher ($x = y \neq z$), $E = 0$; $M_S = \pm 1/2$ KD is the ground state with an easy plane of magnetization along the x,y-directions, giving the separation between the ground and excited KDs = $2D$. When the crystallographic point group symmetry of the metal site is lower than 3-fold ($x \neq y \neq z$) as in **Co-TODA**,[30] $E \neq 0$.[31] The mixing of the $M_S = \pm 1/2$ and $\pm 3/2$ KDs[32,33] gives $2D' = 2(D^2 + 3E^2)^{1/2}$ for the separation between the KDs.[24,29] Here, the $M_S = +1/2$ and $-3/2$ states mix with each other, as the $-1/2$ and $+3/2$ states (Figure 1).[12] The mixed states are labeled ϕ_1 and ϕ_2 for the ground KD and ϕ_3 and ϕ_4 for the excited KD.

The application of memory storage requires the electrons to be in a specific spin state. To prevent spin change, a large, negative D parameter with the easy-axis anisotropy is desirable in SIMs, as this ensures a high energy threshold for spin reverse. Many complexes with the easy-plane anisotropy ($D > 0$) have also shown SIM behaviors with slow magnetic relaxation.[30,34−45] The spin Hamiltonian (SH) in eq 1 has been used to obtain the ZFS parameters and g values from the experiments.[28,29]

$$\hat{H}_S = D(\hat{S}_z^2 - S(S+1)/3) + E(\hat{S}_x^2 - \hat{S}_y^2) + \mu_B g_x B_x \hat{S}_x + \mu_B g_y B_y \hat{S}_y + \mu_B g_z B_z \hat{S}_z \quad (1)$$

where $\hat{S}$ is the spin operator, $S = 3/2$ for Co^{II} ions, μ_B is the electron Bohr magneton, $g_{x,y,z}$ denotes g-tensor components, and B is the applied magnetic field.

Understanding the magnetic properties of Co^{II} complexes and other high-spin systems requires an accurate determination of the ZFS parameters. Direct determination of the ZFS parameters is often challenging.[27] For high-spin Co^{II} complexes with large ZFS (>30 cm^{-1}), for example, there are relatively few spectroscopic methods to determine the ZFS parameters.[27] The ZFS parameters D and E have been typically obtained from fitting data of direct current (DC) magnetic susceptibility data. However, this method is known to be frequently inaccurate. HFEPR,[46] usually operating in the sub-THz frequency range (<30 cm^{-1} for non-Kramers spin systems and <15 cm^{-1} for Kramers spin systems), and magnetic circular dichroism (MCD)[47] have also been used to determine ZFS in metal complexes.[27] Recently, we have employed HFEPR, among others, to determine spin Hamiltonian parameters in $Co(PPh_3)_2X_2$ (X = Cl, Br, I; $2D' \leq 30$ cm^{-1}).[48] The use of HFEPR to measure giant anisotropy in paramagnetic transition-metal complexes, including SIMs, has been reviewed.[27] Far-IR magneto-spectroscopy (FIRMS)[28,48−59] and frequency-domain Fourier transform terahertz EPR[60] are two other direct methods to determine magnetic excited states, including a recent work by Lu, Nelson, and co-workers using terahertz time-domain EPR through a simple tabletop approach to probe the transitions between the spin levels in transition-metal complexes.[61] Brackett and Richards have shown that electronic spin transitions ($\Delta m_S = 0, \pm 1$) between the ground and the excited KDs (Figure 1) are magnetic-dipole-allowed by symmetry and selection rules in far-IR spectroscopy.[49,58] FIRMS has been used to study transitions between the two KDs,[28,48,53−56,62−65] giving, e.g., the energy gap $2D' = 2(D^2 + 3E^2)^{1/2}$ in $S = 3/2$ complexes. For high-spin Co^{II} complexes with large ZFS (>30 cm^{-1}), HFEPR operating in the sub-THz frequency range gives E/D ratio and g values.[28,48,55,56,63−65] The combined use of FIRMS, EPR, and inelastic neutron scattering (INS) has been adopted recently to give ZFS parameters for such complexes.[28,48,55,56,63−65] This approach is still at its early stage, requiring additional studies to understand its scope and applicability.

INS has also been used to probe magnetic as well as phonon properties of chemical compounds,[53,54,66−71] and applications of neutron scatterings in coordination chemistry were recently reviewed.[72] Unlike optical spectroscopies such as IR and Raman, which are governed by symmetry-based selection rules for phonon excitations, INS, which is based on neutron kinetic energy transfer, does not have such selection rules. In other words, INS detects all phonon excitations of molecules in the solid. Here, phonons refer to both intra- and intermolecular vibrations. The phonon spectra obtained by INS help understand spin−phonon couplings in the solid, leading to the relaxation of the molecules from magnetic excited states.[48,54,73] Ab initio density functional theory (DFT) phonon calculations using the Vienna Ab initio Simulation Package (VASP) give calculated INS spectra for comparison with the experimental INS spectra, helping reveal magnetic transitions.[28,48,53,54,73−77] In addition to giving the phonon modes, the calculations by VASP yield spin densities in the molecule (CP), revealing the extent of the spin delocalization.[48,77,78]

Pulsed EPR has been utilized to study magnetic relaxation in metal complexes,[79−83] giving spin−lattice (T_1) and spin−spin

https://doi.org/10.1021/acs.jpcc.2c03083
J. Phys. Chem. C 2022, 126, 13268−13283

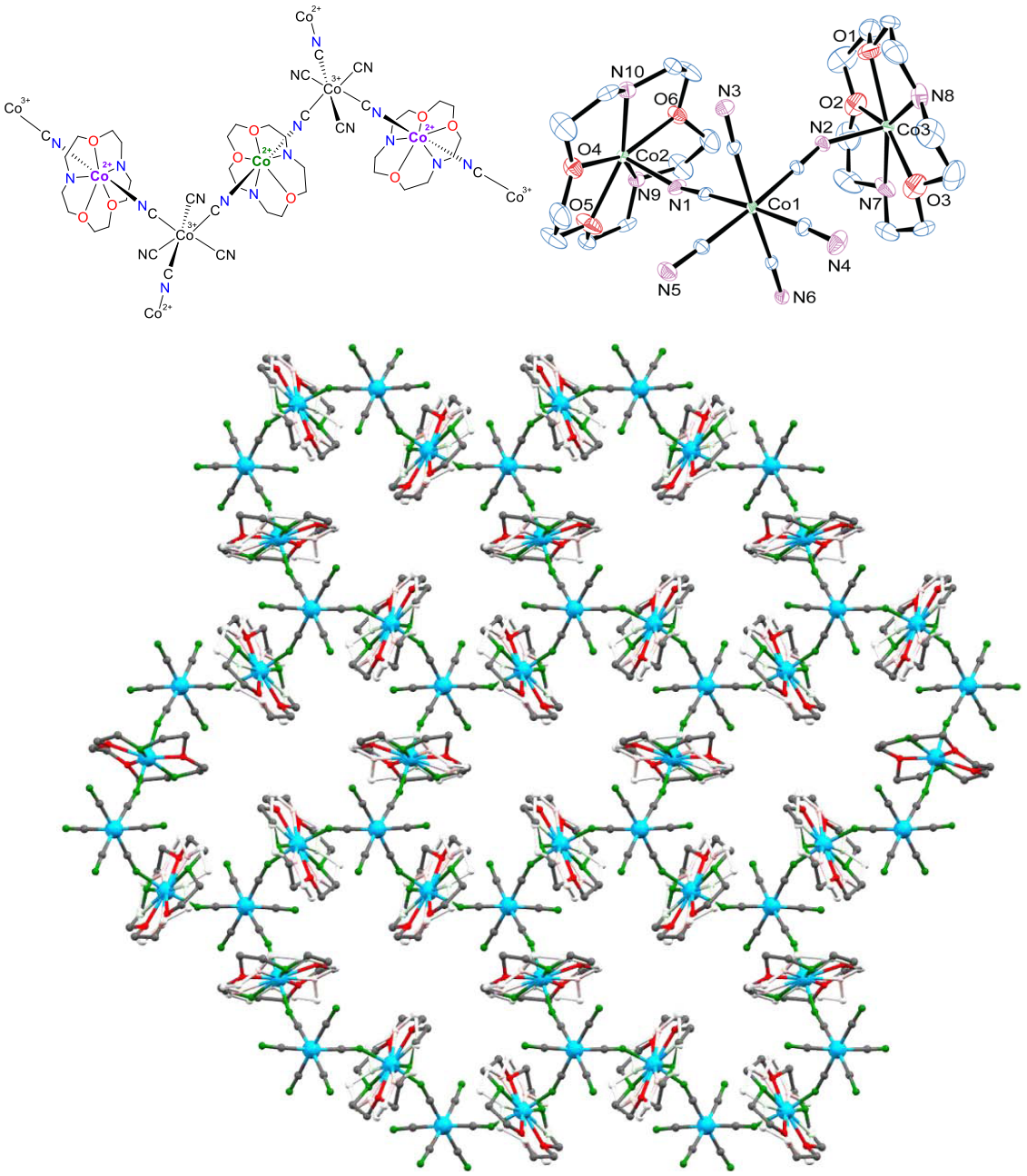

Figure 2. (Top left) $[Co^{III}(CN)_6]_2[Co^{II}(TODA)]_3{\cdot}nH_2O$ (**Co-TODA**). There are two different Co^{II} ions (purple and green color) in the structure. The lattice water molecules are omitted. (Top right) Crystal structure of **Co-TODA** at 15(2) K. Colors: red = O, purple = N, green = Co, blue = C. H atoms and the disordered components of the structure were omitted for clarity. Selected bond lengths and angles are given in Figure S6. (Bottom) Packing structure of **Co-TODA** at 15(2) K, showing the interconnected network with pores in the MOF structure. H atoms and lattice water molecules are omitted for clarity.

(T_2) relaxation times. T_1 quantifies the time of energy transfer from the molecular spin to the lattice or the surrounding environment,[84] while T_2 gives the time of dephasing or decay for the transverse component of the magnetization (M_{xy}). Compounds with long T_2 have been explored as chemical quantum bits (qubits), the basic building block of quantum computers.[80,85−91] For $D > 0$, Co^{II} complexes inside a magnetic field, pulsed EPR may be used to probe the relaxation within the ground KD in Figure 1. Excitation by a microwave pulse leads to the excitation of the molecule from the ground ϕ_1 state to the ϕ_2 state. T_1 and T_2 of the intra-KD relaxation from ϕ_2 to ϕ_1 reveal the roles of spin−lattice and spin−spin interactions in the process.

Two-dimensional (2D) CP **Co-TODA**, $[Co^{III}(CN)_6]_2[Co^{II}(TODA)]_3{\cdot}9H_2O$ (structure in Figure 2), was recently synthesized and found to have SIM properties by some of us.[30] In the CP, there are two slightly different high-spin seven-coordinated Co^{II} ions, each coordinated by a TODA and two CN^- ligands, in addition to a low-spin (diamagnetic) six-coordinated Co^{III} ion. Cyanometallates have been widely used as building blocks to give magnetic materials.[30,92−96] Fitting of direct current (DC) magnetic susceptibility data of **Co-TODA** yielded D = 29.9 and 26.5 cm^{-1} by the PHI and Anisofit2.0 programs, respectively.[30] Alternating current (AC) susceptibility data under 5500 Oe external dc field at 2.0−3.0 K gave the effective energy barrier

https://doi.org/10.1021/acs.jpcc.2c03083
J. Phys. Chem. C 2022, 126, 13268−13283

U_{eff} = 12.6 cm^{-1} and the relaxation time of, e.g., 130 μs at 3.0 K.[30]

We are interested in an in-depth understanding of the magnetic properties of **Co-TODA** with the following aspects: (1) Determination of the CP structure at 15(2) K (near 1.8−3.0 K in which **Co-TODA** reveals the SIM properties) through single-crystal X-ray diffraction to see if there is any phase change from the reported crystal structure at 123 K;[30] (2) Spectroscopic observations of inter- and intra-KD transitions of **Co-TODA** to determine spin Hamiltonian parameters (D, E, and g) of the CP by a combined use of HFEPR and FIRMS; (3) Probe of the inter-KD magnetic transition and phonons by INS with the help of a DFT-calculated INS spectrum; (4) Study of the magnetic anisotropy through electronic structure calculations by complete active space second-order multiconfigurational perturbation theory (CASPT2) and N^- electron valence second-order perturbation theory (NEVPT2); (5) Calculations of spin densities in **Co-TODA** to see, compared with other high-spin Co^{II} compounds, whether there is a correlation between the axial anisotropy (D) values in the compounds (or the CP) and spin densities on the Co^{II} ions; and (6) Determination of spin−lattice (T_1) and spin−spin (T_2) relaxation times for the intra-Kramers $\phi_2 \rightarrow \phi_1$ relaxation by pulsed EPR. Our studies are reported.

EXPERIMENTAL SECTION

The polycrystalline sample of **Co-TODA** was prepared as reported in the literature.[30]

FIRMS Experiment. FIRMS spectra were collected at the National High Magnetic Field Laboratory (NHMFL, Tallahassee, Florida) using a Bruker Vertex 80v Fourier transform infrared (FT-IR) spectrometer coupled with a 17.5 T vertical-bore superconducting magnet. The experimental setup is equipped with a mercury lamp and a composite silicon bolometer (Infrared Laboratories), as an incoherent (sub)-THz radiation source and detector, respectively. The THz radiation is free-space propagating inside the optical beamline, connecting the output of the spectrometer and top of the sample probe. The radiation is then passed through the brass light pipe over a distance of 2.5 m from room temperature to the field center. The probe and beamline are evacuated to eliminate strong parasitic absorptions of the air. The studied samples are the mulls of n-eicosane and powder (∼2 mg) of each complex. Both the sample and the bolometer were cooled by low-pressure helium gas to 5.3(3) K. The spectrum of the THz radiation transmitted through the samples was measured in the spectra between 10 and 720 cm^{-1} (0.3−21.6 THz) with a resolution of 0.3 cm^{-1} (9 GHz), an acquisition time of 3 min, and a scanner speed of 5 kHz. FIRMS spectra of **Co-TODA** were collected four times with different samples, yielding similar results.

HFEPR Experiment. HFEPR spectra were obtained at the NHMFL using the home-built spectrometer based on a 17-T superconducting magnet described previously,[97] and differs from that description only by the use of a low-frequency (8−20 GHz) microwave source complemented by a cascade of amplifiers and multipliers (Virginia Diodes, Charlottesville, VA) to produce higher-frequency harmonics.

INS Experiment. For variable-temperature (VT) INS at VISION, the sample (0.5 g) was sealed in an aluminum container and placed inside the neutron beam at a Vibrational Spectrometer (VISION) at Spallation Neutron Source (SNS), Oak Ridge National Laboratory (ORNL, Oak Ridge, Tennessee). INS spectra of **Co-TODA** were measured at 5.0(5), 25.0(5), 50.0(5), 75.0(5), 100.0(5), 125.0(5), and 150.0(5) K. The design at VISION offers two banks of detectors for both forward (low |**Q**|) and back (high |**Q**|) scattering of neutrons.[98] The phonon population effect was corrected by normalizing the INS intensity at energy transfer ω with $\coth\left(\frac{\hbar\omega}{2k_BT}\right)$.[99]

Electronic Structure Calculations. Electronic structure calculations were conducted by extracting two types of three-core units from the 2D framework complex. For each unit, there are two individual Co^{II} fragments (**Co2** and **Co3** in Figure S1) needed to be calculated while the neighboring Co^{III} ions are diamagnetic. Complete active space second-order multiconfigurational perturbation theory (CASPT2) considering the effect of the dynamic electron correlation based on complete active space self-consistent field (CASSCF) method with MOLCAS 8.4 program package[100] was performed on the basis of single-crystal X-ray-determined geometries of the complex.

For the first CASSCF calculation, the basis sets for atoms are atomic natural orbitals from the MOLCAS ANO-RCC library: ANO-RCC-VTZP for magnetic center ion Co^{II}; VTZ for close N and O atoms; VDZ for distant atoms. The calculations employed the second-order Douglas−Kroll−Hess Hamiltonian, where scalar relativistic contractions were taken into account in the basis set. The effect of the dynamical electronic correlation was applied using CASPT2 based on the first CASSCF calculation. After that, the spin−orbit coupling was handled separately in the restricted active space state interaction (RASSI-SO) procedure. The active electrons in 5 + 5′ active spaces considering 3d double-shell effect include all d electrons [CAS(7 in 5 + 5′)] in the CASSCF calculations. To exclude all of the doubts, we calculated all of the roots in the active space. We have mixed the maximum number of spin-free states that was possible with our hardware (all from 10 quadruplets and 20 from 40 doublets). SINGLE_ANISO[101−103] program was used to obtain zero-field splitting parameters $D(E)$ (cm^{-1}), $\boldsymbol{g}$ tensors, energy levels, magnetic axes, etc., based on the above CASPT2/RASSI-SO calculations.

To deeply analyze the magnetic anisotropies, ORCA 4.2 calculations[104] were performed with complete active space self-consistent field calculations (CASSCF), followed by N^- electron valence second-order perturbation theory (NEVPT2). The spin−orbit coupling (SOC) operator used was the efficient implementation of the multicenter spin−orbit mean-field (SOMF) concept developed by Hess et al.[105] The spin−spin contributions (SSC) to the D values were also included although they are very small for our complex. The NEVPT2[106−109] calculation both with seven 3d electrons in five Co 3d-based orbitals [CAS(7, 5 + 5′)] including 3d double-shell effects was performed on **Co2** and **Co3**. In the calculations, the orbitals were determined for the average of 10 S = 3/2 and 40 S = 1/2 roots. All calculations were performed with triple-ζ with one polarization function def2-TZVP[110−112] basis set for all atoms.

DFT Calculations of INS Spectrum and Spin Densities. Spin-polarized density functional theory (DFT) calculations of the **Co-TODA** compound were performed using the Vienna Ab initio Simulation Package (VASP).[113] The calculation used projector augmented wave (PAW) method[114,115] to describe the effects of core electrons and Perdew−Burke−Ernzerhof

https://doi.org/10.1021/acs.jpcc.2c03083
J. Phys. Chem. C 2022, 126, 13268−13283

(PBE)[116] implementation of the generalized gradient approximation (GGA) for the exchange-correlation functional. The energy cutoff was 600 eV for the plane-wave basis of the valence electrons. The lattice parameters and atomic coordinates from the original paper[30] were used as the initial structure. Ideally, the partial occupancy and structure disorder should be accounted for by creating a supercell and assigning the ligands to each possible configuration according to the occupancy probability. This is, however, too costly for the already large unit cell (volume >3500 Å^3). As an approximation, this procedure was done within the unit cell, resulting in the same periodicity with internal disorder (loss of symmetry). The electronic structure was calculated at the Γ point only. The total energy tolerance for electronic energy minimization was 10^{-8} eV, and for structure optimization, it was 10^{-7} eV. The maximum interatomic force after relaxation was below 0.001 eV Å^{-1}. The optB86b-vdW functional[117] for dispersion corrections was applied, and a Hubbard U term of 3.32 eV[118] was applied to account for the localized 3d orbitals of Co. The interatomic force constants were calculated by the finite displacement method, and the vibrational eigenfrequencies and modes were then calculated using Phonopy.[119] The OCLIMAX software[76] was used to convert the DFT-calculated phonon results to the simulated INS spectra.

Pulsed EPR Experiment. Pulsed X-band EPR experiments were performed on a Bruker E680 spectrometer (Billerica, MA) operating at a microwave frequency of 9.5 GHz at the NHMFL. Echo detection and T_1 and T_2 relaxation times were collected using a dielectric ER4118X-MD-5 resonator equipped with an Oxford CF-935 helium flow cryostat. The temperature was controlled and monitored using an Oxford Instrument ITC503 temperature controller. The 4-mm outer-diameter EPR tubes were used to load samples. The experiments were conducted in the temperature range of 5(1)−30(1) K. Echo-detected field swept spectra were obtained by measuring the Hahn echo intensity ($\pi/2-\tau-\pi-\tau-$echo) as a function of transverse field. The time delay (τ) between two detection pulses was 200 ns. Echo detection was swept from 100 to 10 000 G magnetic field. T_1 was measured using an echo-detected inversion recovery pulse sequence ($\pi-\tau_1-\pi/2-\tau-\pi-\tau-$echo). T_2 was measured using a standard two-pulse Hahn echo sequence ($\pi/2-\tau-\pi-\tau-$echo). The lengths of the $\pi/2$ and π pulses were 16 and 32 ns for all experiments, respectively.

RESULTS AND DISCUSSION

Single-Crystal Structure of Co-TODA at 15(2) K. Determination of the crystal structure of **Co-TODA** at 15(2) K by X-ray diffraction was prompted by the following two considerations: (1) Reported SIM behaviors of **Co-TODA** (and many other SMMs) are displayed at 15(2) K or below, while its reported crystal structure was determined at 123 K.[30] (2) While the structure at 123(2) K shows two Co^{II} centers, neither FIRMS nor HFEPR, discussed below, resolved the transitions from the two Co^{II} centers in **Co-TODA**. Thus, it is desirable to rule out a phase change between 123(2) and 15(2) K.

The structure at 15(2) K determined by synchrotron X-ray diffraction is similar to that at 123 K (Figure 2, right). The shortest Co^{II}···Co^{II} distance is 7.52 Å, while the longest Co^{II}···Co^{II} distance is 15.4 Å with an interlayer separation of 9.18 Å between the Co^{II} ions. Each diamagnetic Co^{III} ion acts as a spacer between the Co^{II} ions, making each Co^{II} unit as a SIM. Both Co^{II} ions, **Co2** and **Co3**, are coordinated by the five atoms (three N and two O atoms) of a TODA ligand and two N atoms of the CN$^-$ ligands in similar pentagonal bipyramidal geometries. Continuous shape measures (CShM) were performed on the two Co^{II} centers in the 15(2) K structure to determine their deviations from the ideal (D_{5h}) geometry. The CShM values of **Co2** and **Co3** show deviations of 0.791 and 0.410 from 0, respectively. With similar geometries, the magnetic properties of the two different Co are expected to be comparable.

Additional plots of the 15(2) K crystal structure in **Co-TODA**, showing its CP features, are given in the Supporting Information (SI). Variable-temperature (VT) HFEPR was performed to observe potential changes to the magnetic properties between 5 and 150 K due to the potential phase change. The VT-HFEPR results will be discussed below.

Studies of the Magnetic Transitions by FIRMS and HFEPR to Determine Spin Hamiltonian Parameters. *FIRMS.* As indicated earlier, the FIRMS experiment was used to probe dominant inter-Kramers transitions from ϕ_1 to ϕ_3 and ϕ_4 (Figure 1). The experiments were performed several times at 5.3(3) K under magnetic field ranging from 0.000(2) to 17.000(2) T with a 1 T step. Figure 3(top) shows a

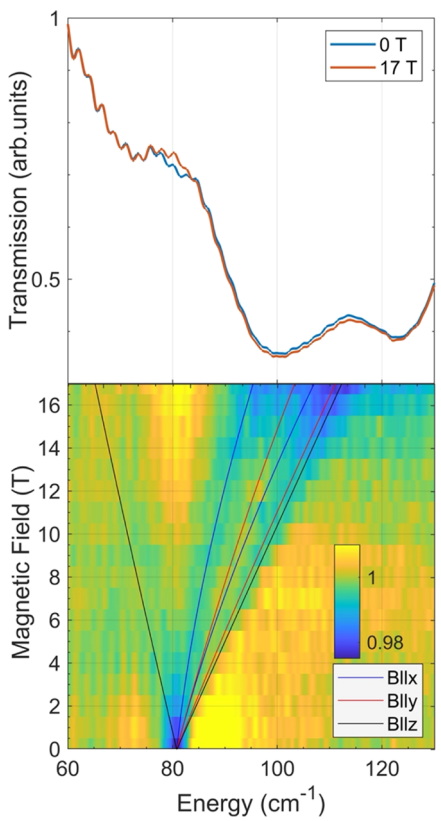

Figure 3. (Top) Transmittance line plot of FIRMS data at 5.3(3) K. (Bottom) 2D FIRMS plot showing the zero-field magnetic transition originating from 80.4(1.0) cm^{-1} and its evolution at applied high magnetic fields. The blue, red, and black lines are simulated transitions, using EasySpin on MATLAB,[120] when the magnetic field is applied along the x-, y-, and z-axes of the [D,E] tensor, respectively. The ZFS parameters used in the simulations are D = +38.3(1.0) cm^{-1}, |E| = 7.3(1.0) cm^{-1}, and g = [2.33(6), 2.33(6), 2.06(6)], as discussed below in the HFEPR section. The 2D FIRMS plot was obtained from data normalized to the reference spectrum, which is the average spectrum for all magnetic fields.

https://doi.org/10.1021/acs.jpcc.2c03083
J. Phys. Chem. C 2022, 126, 13268−13283

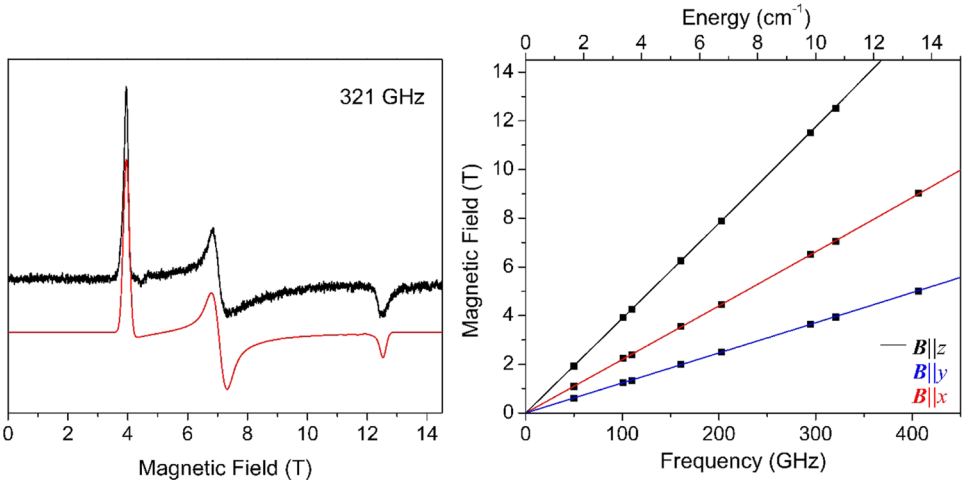

Figure 4. (Left) HFEPR spectrum of **Co-TODA** at 10(1) K and 321 GHz (black trace) and its simulation (red trace) using the following SH parameters: D = +38.3(1.0) cm^{-1}, $|E|$ = 7.3(1.0) cm^{-1}, g = [2.33(6), 2.33(6), 2.06(6)]. (Right) 2D map (magnetic field vs frequency/energy) of turning points in HFEPR spectra of **Co-TODA** at 10(1) K. Squares are experimental points, while lines were simulated using best-fit SH parameters. (The D and E values were chosen such that $2D'$ agrees with the ZFS transition that was found in FIRMS).

transmittance plot of the FIRMS data. The data were collected at each magnetic field separately and then normalized to a reference, which is an average of all transmission spectra. The purpose of the normalization is to eliminate instrumental arbitrations or artifacts as well as the nonmagnetic spectrum background. A comparison of the 0 and 17 T transmittance plots (Figure 3, top) did not clearly reveal a magnetic peak in the 0 T plot. However, a major change of ∼2% in intensity between the 0 and 17 T spectra (Figure 3, top) is observed around 80.4(1.0) cm^{-1}, while spectra match each other beyond this spectral range. In Figure 3 (bottom), a colored two-dimensional (2D) FIRMS plot was obtained through a normalization process. In this plot, the intensity in the blue region reveals the magnetic transitions. The FIRMS and HFEPR (discussed below) do not have enough resolution to resolve the magnetic transitions from the two Co^{II} centers in the CP in powder form. The blue region at ca. 78−83 cm^{-1} is broad, suggesting that transitions from both Co^{II} centers are in the 2 cm^{-1}-wide range. The transitions from two different Co^{II} centers in **Co-TODA** cannot be distinguished in Figure 3 (bottom) in part because the transition is weak. Repeated FIRMS experiments to resolve the transitions from the two Co^{II} centers did not work. The energy separation between the two Kramers doublets (Figure 1) is $2D'$ = 80.4(1.0) cm^{-1}. The result from FIRMS, combined with those from HFEPR, give the SH parameters discussed below.

For S = 3/2 compounds (or CPs) with rhombic E ($\neq$0) parameters, such as **Co-TODA** here, mixing of the two spin states (Figure 1) makes both inter-KD transitions from ϕ_1, $\phi_1 \rightarrow \phi_3$ and $\phi_1 \rightarrow \phi_4$, allowed inside a magnetic field. The zero-field splitting is directly observed at 80.4(1.0) cm^{-1} (Figure 3, bottom). The simulated transitions in Figure 3 (bottom) were generated using EasySpin[120] on MATLAB and D = +38.3(1.0) cm^{-1}, $|E|$ = 7.3(1.0) cm^{-1}, and g = [2.33(6), 2.33(6), 2.06(6)]. As the magnetic field increases, the two transitions from ground state $\phi_1 \rightarrow \phi_3$ and $\phi_1 \rightarrow \phi_4$ split, each along the $B||x$, $B||y$, and $B||z$ directions of the magnetic anisotropy tensor. One $B||z$ transition is red-shifted to lower energy (Figure 3). The other $B||z$ transition and two $B||x$ and $B||y$ transitions each are blue-shifted with increasing field. One $B||x$ transition matches an observed trace in Figure 3 (bottom) well. Another observed trace appears to follow one simulated $B||y$ and $B||z$ transitions. These lines restrict the area of the resonance frequencies, which are smeared in the magnetic field due to the arbitrary orientation of the microcrystalline in the powder sample. The FIRMS spectra and EasySpin simulations are similar to the reported FIRMS spectra of Co(acac)$_2$(H$_2$O)$_2$ and simulations of the spectra, which also give one redshift and five blueshift traces for the $\phi_1 \rightarrow \phi_3$ and $\phi_1 \rightarrow \phi_4$ transitions.[28] The simulations in the current work gave reasonable fits to the experimental data, which further support the direct observation of the zero-field splitting at 80.4(1.0) cm^{-1} as well as the Zeeman splitting that occurs at a higher magnetic field.

No spin−phonon coupling was observed in FIRMS involving the magnetic transitions from 80.4(1.0) cm^{-1}, although there is a strong far-IR peak at ∼98 cm^{-1}, which may be too far from 80.4(1.0) cm^{-1} to show spin−phonon coupling at 0 T. The magnetic transition at 80.4(1.0) cm^{-1} in FIRMS is not strong. In addition, the CP structure leads to unique vibrational/phonon features (which appear to be different from those of molecular compounds).[121] For example, rotations of organic linkers in MOFs may be hindered. Trampoline-like motions were observed recently in a low-symmetry MOF, which was believed to be a potential source of negative thermal expansion of the MOF.[121] However, to understand why spin−phonon coupling in **Co-TODA** was not observed in FIRMS requires separate studies including computations similar to those reported recently for ionic and molecular compounds.[80,122−125]

INS was also performed to determine the inter-Kramers transition and phonon features in **Co-TODA** that are discussed below.

HFEPR. The HFEPR experiment was used to probe intra-Kramers transition ϕ_1 to ϕ_2 (Figure 1). For each frequency used for a powder sample of **Co-TODA**, three peaks at different magnetic fields: $B||x$, $B||y$, and $B||z$, are expected.

The experiment was conducted at 10(1) K with various set frequencies and variable magnetic field. **Co-TODA** produced a clear HFEPR pattern at any frequency, showing three peaks (turning points) when pressed into a pellet with *n*-eicosane. The spectrum was simulated using the SH parameters in the caption of Figure 4 with the assumption of powder distribution

https://doi.org/10.1021/acs.jpcc.2c03083
J. Phys. Chem. C 2022, 126, 13268−13283

of crystallites in the sample. The simulated spectrum agrees very well with the experimental one. It is characteristic of a high-spin Co^{II} ion with positive D, i.e., easy-plane anisotropy, and pronounced rhombicity (E) of the ZFS tensor. Figure 4 (left) shows a spectrum at 10(1) K and 321 [or 321.000(2)] GHz with its simulation.

The separation of B_x and B_y turning points in the HFEPR spectra could also be a result of the g-anisotropy (g_x not equal to g_y). However, simulations show that, for the g-anisotropy to reproduce that separation, the g-values would have to be physically unrealistic. The actual E parameter should thus be understood as being $0 \ll |E| \leq 7.3(1.0)$ cm^{-1} and D as $+38.0(1.0) \leq D \ll +40.2(1.0)$ cm^{-1}. That is, the $|E|$ and D values are much closer to 7.3(1.0) and +38.0(1.0) cm^{-1}, respectively, than to 0 and +40.2(1.0) cm^{-1}.

Due to the large rhombicity ($E \gg 0$) in **Co-TODA**, there is a significant mixing of the $M_S = \pm 1/2$ and $\pm 3/2$ spin states, giving, e.g., $\phi_1 = -a|-1/2\rangle + b|+3/2\rangle$ and $\phi_2 = -a|+1/2\rangle - b|-3/2\rangle$ for the lower-energy KD [mixing coefficients: $a = \cos\beta$, $b = \sin\beta$, $\tan 2\beta = \sqrt{3}\,(E/D)$], as shown in Figure 1. Thus, the Zeeman splitting is a function of both g and the mixed spin states. Using the $D' = (D^2 + 3E^2)^{1/2}$ value from FIRMS, a simulation of the 2D map of turning points in Figure 4 (right) gave the values of the spin Hamiltonian (SH) parameters D, E, and $\boldsymbol{g}$ [g_x, g_y, g_z]. The simulations assume that the g-tensor is axial, which we do not know since E and g-rhombicity are interrelated. We can only state that the $|E/D| = 0.19$ ratio represents the maximum value. With the combined data from FIRMS and HFEPR, we were able to quantify the values of D, E, and g in the spin Hamiltonian as well as determine the inter-Kramers transition energy of the CP.

The single-crystal structure of **Co-TODA** at 123(2) K shows two different Co^{II} centers, while both FIRMS and HFEPR data at 5−10 K, using powder samples, did not resolve the transitions from the two Co^{II} centers in **Co-TODA**. Repeated attempts to synthesize the CP only yielded powders or small crystals not large enough for single-crystal FIRMS and HFEPR studies. The single-crystal structure of **Co-TODA** at 15(2) K, discussed earlier, is similar to that at 123(2) K, ruling out a phase change between the two temperatures. In other words, the two different Co^{II} centers exist at both 15(2) and 123(2) K. We have decided to conduct VT HFEPR at several temperatures between 5(1) and 150(1) K to reveal potential changes in the magnetic properties of the molecule at the different temperatures. Figure 5 shows the VT HFEPR graph at a set frequency of 273 [or 273.000(2)] GHz. The characteristics of all three visible EPR patterns did not change as the temperature decreased. The VT HFEPR results are consistent with the single-crystal X-ray diffraction results, which showed no phase transition between 5(1) and 150(1) K. Therefore, there are no changes to the magnetic characteristics of **Co-TODA** at the low temperature.

It is noted that both the current FIRMS/HFEPR spectroscopies and earlier DC susceptibility data fitting[30] show that **Co-TODA** has the easy-plane anisotropy, although the current spectroscopic studies give direct determination of the D and E values. The easy-plane anisotropy ($D > 0$) obtained from HFEPR here is supported by the ab initio calculations discussed below. Easy-axis anisotropy ($D < 0$) was considered to be an important criterion for SIMs because it favors high $|M_S|$ states energetically.[126] In a classical picture, for molecules with the easy-plane anisotropy, there is no (when $E = 0$) or a small (when $E \neq 0$) barrier for spin reversal because of the

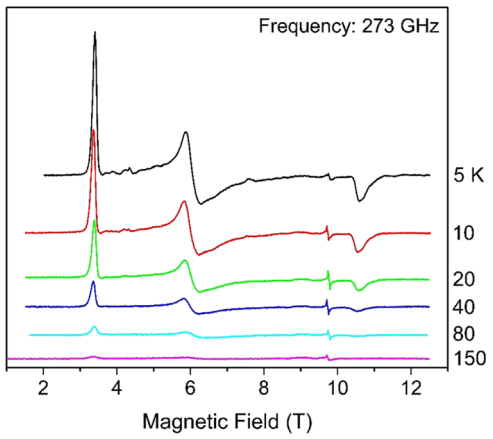

Figure 5. VT HFEPR spectra at 273 GHz with temperatures ranging from 5(1) to 150(1) K. The narrow resonance at ca. 9.8 T is due to an unidentified $S = 1/2$ impurity.

condition $|E| = D/3$.[126] In addition, spin tunneling rates are expected to be high.[126] Both factors contribute to the loss of magnetic memory. However, many complexes with the easy-plane anisotropy,[34−45] including **Co-TODA** here,[30] have shown SIM behaviors with slow magnetic relaxation. Using $Co(acac)_2(H_2O)_2$ ($acac^-$ = acetylacetonate) as a model, Gómez-Coca and co-workers have found that the slow relaxation in such systems is a general consequence of time-reversal symmetry that hinders direct spin−phonon processes regardless whether the complexes have the easy-plane or easy-axis anisotropy.[126] It is also noted that the reported AC susceptibility measurements of **Co-TODA** at 2.0−3.0 K give $U_{eff} = 11$ cm^{-1},[30] which is significantly lower than $+38.0(1.0) \leq D \ll +40.2(1.0)$ cm^{-1} determined spectroscopically here.

INS Studies of the Inter-KD Transition and Phonon Properties. INS spectra give complete phonon spectra of the sample, which may help understand the phonon properties of the CP. In addition, INS may show magnetic transitions in the sample. There are generally two types of interactions between incident neutrons and a sample in the INS process. The neutrons interact with the atomic nuclei of the sample, leading to the excitation of phonons. The neutrons (spin = 1/2) also interact with the magnetic field of the sample created by its unpaired electrons, leading to magnetic excitations.

Phonons of molecular crystals include both internal and external modes.[73,127] Internal mode or (intramolecular) vibration is caused by the distortion of atoms in a molecule as well as a slight shift in the molecular center of mass. External mode (or lattice vibration) is that of the lattice with little to no internal distortion of the molecule. All phonon modes, however, exhibit features of both internal and external modes. Phonons in this study refer to both external and internal modes in the solid. Variable-temperature (VT) INS may be used to differentiate the magnetic and phonon transitions. Because electrons and phonons are fermions and bosons, respectively, they will have different temperature profiles, making it possible to use Bose-corrected VT INS to distinguish magnetic transitions from those of phonons.

Current INS studies were conducted using a vibrational spectrometer (VISION) at ORNL. The INS work was performed by sealing 0.5 g of sample in an aluminum container under helium. The spectra were measured at 5.0(5), 25.0(5), 50.0(5), 75.0(5), 100.0(5), 125.0(5), and 150.0(5) K for 1 h at each temperature. Bose-corrected INS

https://doi.org/10.1021/acs.jpcc.2c03083
J. Phys. Chem. C 2022, 126, 13268−13283

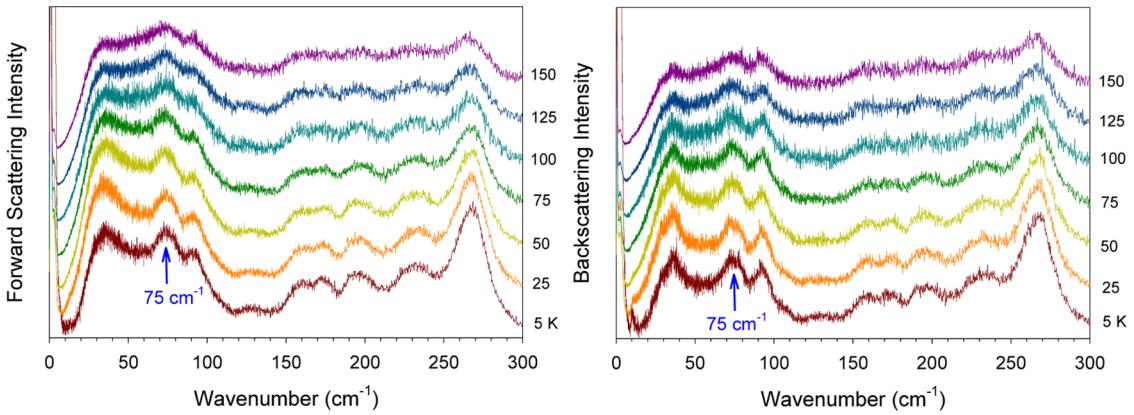

Figure 6. Bose-corrected INS spectra collected at VISION. (Left) Forward scattering; (right) Backscattering.

spectra of forward-scattering data and backscattering data are given in Figure 6. Since phonons are bosons following the Bose–Einstein statistics,[36,53,54,67,70,71,128] the Bose correction applies a frequency- and temperature-dependent normalization factor such that INS spectra measured at different temperatures are brought to a similar level for comparison. In other words, the spectrum is divided by the phonon population factor, which facilitates the comparison of the various spectra collected at different temperatures.

Phonon features at different temperatures in Bose-corrected spectra are expected to have similar profile and baseline intensity. The magnetic transition from electrons, which are fermions, does not follow the expected temperature dependence for phonons. A broad peak was observed at ~75(2) cm^{-1} in the INS spectrum at 5.0(5) K, which is more intense in the forward scattering (Figure 6, left) than in the backscattering spectrum at 5.0(5) K (Figure 6, right), when, e.g., compared with the peak to its right [at ~94(1) cm^{-1}]. In INS, magnetic transitions are stronger in the forward scattering (with smaller magnitudes of the momentum transfers, $|\boldsymbol{Q}| = |\boldsymbol{k}_i - \boldsymbol{k}_f|$, where $\boldsymbol{k}_i$ and $\boldsymbol{k}_f$ refer to the momenta of the incoming and outgoing neutrons, respectively) than in the backscattering spectra, while phonon transitions are weaker in the forward-scattering than in the backscattering spectra.[72] Thus, it is likely that the broad peak at ~75(2) cm^{-1}, extending to >82 cm^{-1}, contains the contribution from the magnetic transition. That is, overlapping peaks of magnetic and phonon transitions at ~75(2) cm^{-1} make the peaks more intense in the forward-scattering spectrum at 5.0(5) K than that in the backscattering spectrum. However, the broad, likely overlapping peaks at ~75(2) cm^{-1} from a powder sample of **Co-TODA** prevents definitive assignment of the magnetic contribution to the peaks. The spectrum shows two phonon features between 70 and 100 cm^{-1}. The phonon features around the region of the observed magnetic transition [80.4(1.0) cm^{-1} from FIRMS] can potentially lower the relaxation time of the spins due to the phonon acting as an external perturbation to the system. Even though phonons are found around the region of the magnetic transition, no phonon coupling was observed in FIRMS.

Density functional theory (DFT) calculations of the phonon INS spectrum of **Co-TODA** were conducted using VASP. The goal of the calculations is to compare the calculated phonon INS spectrum to the experimental one so a magnetic transition in the experimental INS spectra, which is not in the calculated phonon INS spectrum, may be revealed. Due to the complexity of the crystal structure of the **Co-TODA** and the disorder of the TODA ligands, the symmetry of the CP was lowered to *P*1 in the calculations. Since the calculations were not conducted in the original, higher symmetry of $P2_1/c$ (no. 14), phonon modes were not assigned symmetries. The calculated INS spectrum in the range of 10–4000 cm^{-1} is given in Figure S17, in comparison with the experimental INS at 5 K. The calculated and experimental INS spectra match fairly well, considering that the magnetic transition at 80.4(1.0) cm^{-1} overlaps with phonon peaks around 75(2) cm^{-1}.

Computational Studies of the Magnetic Anisotropy in Co-TODA. With the determination of the easy-plane anisotropy in **Co-TODA** by both FIRMS/HFEPR spectroscopies and DC susceptibility data fit, we have conducted ab initio studies to understand the anisotropy.

There are two Co^{II} ions, **Co2** and **Co3**, in the crystal structure of **Co-TODA**, both coordinated by TODA ligands (Figure 2). The calculated molecular structures of individual Co^{II} fragments are given in Figure S1. The energy differences between the lowest two spin-free states (Table S1) of **Co2** and **Co3** are both much larger than those between the lowest two spin–orbit states (Table S2), and the compositions of the ground spin–orbit states are almost entirely from the ground spin-free states. Thus, we can use ZFS parameters *D* and *E* to depict their magnetic anisotropies.

The calculated *D*, *E* (cm^{-1}), and $\boldsymbol{g}$ (g_x, g_y, g_z) tensors for **Co2** and **Co3** using CASPT2 and NEVPT2 with MOLCAS 8.4[100] and ORCA 4.2,[104] respectively, are shown in Table S3, where the *D* values obtained from NEVPT2 are more consistent with the experiments compared with those from CASPT2. Figure S2 shows calculated orientations of the local magnetic axes (g_x, g_y, g_z) on **Co2** and **Co3** in their ground spin–orbit states using CASPT2/RASSI-SO with MOLCAS 8.4. To analyze magnetic anisotropies deeply, we gave the contributions of the excited states to *D* values for **Co2** and **Co3** in Table S4 using NEVPT2 with ORCA 4.2. The dominant contributions to the positive *D* values were from the two close quartet states, particularly the third and fourth quartet states for both **Co2** and **Co3**. The calculations yield positive *D* values, which are consistent with the geometries around the Co^{II} ions and easy-plane anisotropies (g_x, $g_y > g_z$). The molecular coordination frame was chosen so that the *Z* axis is along the numerically largest eigenvalue of the *D*-tensor and the *X* and *Y* axes accordingly to the other two. The following discussion of Co d-atomic orbitals (d-AOs) is classified in accordance with this frame. The calculated relative energies (cm^{-1}) of ligand field one-electron states (on the basis of d-AOs) for **Co2** and **Co3** using

https://doi.org/10.1021/acs.jpcc.2c03083
J. Phys. Chem. C 2022, 126, 13268–13283

NEVPT2 with ORCA4.2 are shown in Table S5 according to the ab initio ligand field theory (AILFT)[129,130] analysis. The CASPT2 calculations gave the D values for **Co2** and **Co3** as 30.5 and 43.0 cm^{-1}, respectively. The experimental value of D from HFEPR [$+38.0(1.0) \leq D \ll +40.2(1.0)$ cm^{-1}] is between the calculated D values of **Co2** and **Co3** from CASPT2.

The magnetic susceptibility of **Co-TODA** was calculated using CASPT2/RASSI-SO with MOLCAS 8.4. The calculated plots of magnetic susceptibilities vs temperatures for both **Co2** and **Co3** are shown in Figure S3, giving the susceptibility value of 1.5−1.7 cm^3 mol^{-1} K near 0 K that plateaus around 2.5 cm^3 mol^{-1} K at 300 K. The calculated magnetic susceptibilities of **Co2** and **Co3** are alike, supporting that the two Co^{II} centers have close characteristics. The calculated plots are similar to those from the earlier experiments.[30] For example, the experimental magnetic susceptibility value, which does not distinguish the contributions from **Co2** or **Co3**, is 1.37 cm^3 mol^{-1} K at 2 K, while plateauing around 2.48 cm^3 mol^{-1} K at room temperature. Therefore, the calculated magnetic susceptibility values are agreeable with the experimental data.[30]

For **Co2** and **Co3**, the most destabilized ligand field is the singly occupied state composed of practically pure d_{z^2} AOs. The orbital energies computed for the ground states are shown in Figure S4, where the ground states for **Co2** and **Co3** are both multideterminant with prevailing (62.2 and 84.1%, respectively) contribution of $(d_{yz})^1(d_{xz})^2(d_{xy})^1(d_{x^2-y^2})^2(d_{z^2})^1$ and $(d_{yz})^1(d_{xz})^2(d_{xy})^1(d_{x^2-y^2})^2(d_{z^2})^1$, and are mixed with another with the weightages of 13.3 and 12.1%, respectively. For **Co2**, the major contributions to D are from the ground to the third and fourth excited-state transitions ($d_{xz} \rightarrow d_{z^2}$ and $d_{x^2-y^2} \rightarrow d_{z^2}$, respectively). The positive sign of the D parameter is attributed to these transitions that occur between orbitals with different magnetic quantum number (m_l) values.[23,131] In the case of **Co3**, as it is similar to **Co2**, the largest contributions to D are also from the ground to the third and fourth excited-state transitions ($d_{x^2-y^2} \rightarrow d_{yz}$ and $d_{x^2-y^2} \rightarrow d_{z^2}$, respectively). Since these orbitals also have different m_l values, the contributions to the D value are positive, in complete agreement with the experiments.

The multideterminant wavefunctions of the selected excited states having important contributions to D tensor are shown in Figure S5, where all of the excited states are composed of several configurations, indicating the presence of the unquenched orbital angular momentum. The calculated $\chi_M T$ vs T plots are shown in Figure S3. The calculated orientations of the g_x, g_y, and g_z in the ground spin−orbit states on Co^{II} ions of **Co2** and **Co3** are shown in Figure S2.

Calculated Spin Densities and a Correlation with the *D* Parameter. Spin density calculations were performed using Vienna Ab initio Simulation Package (VASP) with the projector augmented wave (PAW)[114,115,132,133] method and the local density approximation (GGA)[116] + U (U = 4.4 eV)[134,135] exchange-correlation functional. Spin density calculation is used to study the localization of spin in the metal ions as well as the ligands. The calculations do not include the spin densities that reside in the bonds, but rather just the densities in individual atoms. The range of spin densities for each atom type is presented in Table 1. Detailed spin densities are given in Table S9.

The results show that the spin densities are mostly concentrated on the Co^{II} ions, containing 2.68−2.69 (89.3−89.7%) of the three unpaired electrons on the metal ions, while the rest are dispersed on the ligands and the diamagnetic Co^{III} ions. We recently found that, among four Co^{II} complexes $Co(PPh_3)_2X_2$ (X = I, Br, Cl) and $Co(acac)_2(H_2O)_2$ (acac = acetylacetonate), the larger the spin density on a metal ion, the larger the ZFS is in the complex,[48] as summarized in Table 2. **Co-TODA** in the current work [D' = 40.2(1.0)] follows the trend (Table 2). Its spin densities of 2.68−2.69 on the Co^{II} ions and D' = 40.2(1.0) are both lower than those of $Co(acac)_2(H_2O)_2$ but higher than those of $Co(PPh_3)_2X_2$ (X = I, Br, Cl) (Table 2).

In both $Co(acac)_2(H_2O)_2$ and **Co-TODA**, only light N and O atoms (in the second row of the periodic table) are bound to the Co^{II} ions with six- and seven-coordination, respectively. For **Co-TODA**, seven N,O atoms (and other atoms in the ligands) share the spin densities from the three unpaired electrons, while in $Co(acac)_2(H_2O)_2$, six O atoms bound to the Co^{II} ion (and other atoms of the ligands) share the spin densities. Perhaps the different coordination numbers in $Co(acac)_2(H_2O)_2$ and **Co-TODA** is one contributor to the spin density differences between the two. In $Co(PPh_3)_2X_2$ (X = I, Br, Cl), the halogen atoms in the third, fourth, and fifth rows of the periodic table have higher spin densities [6.69×10^{-2} (Cl), 6.85×10^{-2} (Br), and 6.01×10^{-2} to 6.39×10^{-2} (I) in the three complexes, respectively[48]] than, e.g., those on N and O atoms in **Co-TODA**.

It should be pointed out that the number of complexes here (five in Table 2) is limited, and different DFT programs may give different calculated spin densities. Additional studies are needed to see if there is a correlation between the spin densities and magnitudes of ZFS.

Table 1. Calculated Spin Densities for Atoms in a Unit Cell of Co-TODA[a]

atoms	ranges of spin densities
Co^{II}	2.69
Co^{III}	0.01
O	2.15×10^{-2} to 3.57×10^{-2}
N of TODA	4.31×10^{-2} to 4.33×10^{-2}
N of CN^-	-1.14×10^{-4} to -1.02×10^{-4}
	2.11×10^{-4} to 1.92×10^{-2}
C of CN^-	-2.03×10^{-4} to -1.18×10^{-4}
	7.89×10^{-5} to 7.23×10^{-3}
C of TODA	-8.96×10^{-4} to -2.89×10^{-4}
	7.62×10^{-5} to 1.81×10^{-3}
H	-3.14×10^{-4} to -1.2×10^{-7}
	2.00×10^{-8} to 2.04×10^{-3}
total	17.616 (2.936 per SBU[b])

[a]Ranges of spin densities are listed for O, N, C, and H atoms due to the large number of atoms present in the unit cell. [b]SBU = secondary building unit.

Table 2. Correlation between Calculated Spin Densities on the Co^{II} Ions and ZFS Parameters of the Co^{II} Complexes/CP

complexes	spin densities on the Co^{II} ions (and percentage of three unpaired electrons)	D' values (cm^{-1})
$Co(PPh_3)_2I_2$	2.553 (85.1%)	13.63(10)
$Co(PPh_3)_2Br_2$	2.570 (85.7%)	13.83(2)
$Co(PPh_3)_2Cl_2$	2.585 (86.2%)	14.89(2)
Co-TODA	2.68−2.69 (89.3−89.7%)	40.2
$Co(acac)_2(H_2O)_2$	2.81 (93.7%)	57.0

https://doi.org/10.1021/acs.jpcc.2c03083
J. Phys. Chem. C 2022, 126, 13268−13283

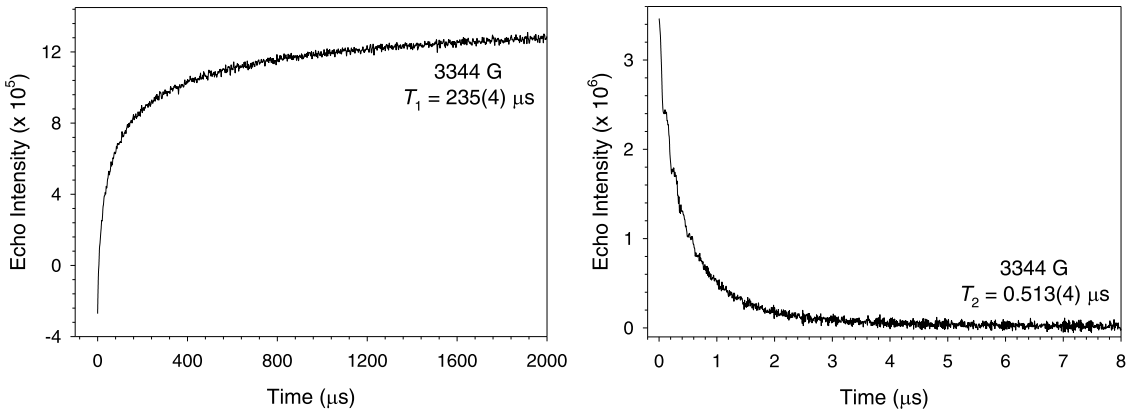

Figure 7. Graphs of the echo intensity from pulsed X-band EPR at 5(1) K vs time: (left) echo inversion recovery experiment; (right) Hahn echo decay experiment. External magnetic field = 3344(1) G.

Studies of Spin−Lattice (T_1) and Spin−Spin (T_2) Relaxation Times in the Ground KD by Pulsed X-Band EPR. Pulsed X-band EPR was used to probe the spin−lattice and spin−spin relaxation times T_1 and T_2 after the Co^{II} centers are excited from ϕ_1 to ϕ_2 (Figure 1). In other words, pulsed EPR here provides relaxation times for the intra-KD transition inside a magnetic field. The two relaxation times are intrinsic magnetic properties of **Co-TODA**.

T_1 quantifies the time of energy transfer from the molecular spin to the lattice.[84] Using the technique of echo inversion recovery, a pulsed wave at 180° is applied inside a field,[136,137] leading to the flipping of the magnetization ($\boldsymbol{M}_z$) from $+z$ to $-z$ with a higher energy. Afterward, the flipped spin will undergo spin−lattice relaxation to return to $+z$, releasing energy to the environment through spin−lattice relaxation. $M_z(t)$, magnetization along z at different times (t) after the 180° pulse, is measured. T_1 is the time for $M_z(t)$ to reach 63% of its maximum value, $M_z(0)$, as shown in eq 2.[138,139] T_1 is also the time at which the spins relax back to the Boltzmann equilibrium state at a given temperature after the removal of the external magnetic field. T_1 is an important magnetic property of a compound or CP, e.g., for the relaxation from ϕ_2 to ϕ_1 in **Co-TODA**.

$$M_z(t) = M_z(0)[1 - 2\exp(-t/T_1)] \quad (2)$$

where $M_z(0)$ and $M_z(t)$ are the axial components of the magnetization vector at time = 0 and t, respectively, and T_1 is the spin−lattice relaxation time.

Spin−spin relaxation is the process where the transverse component of the magnetization ($\boldsymbol{M}_{xy}$) dephases or decays. According to Bloch, this process follows first-order kinetics resulting in the exponential decay.[138] T_2 is the time it takes for the traverse magnetization to fall to 37% of its initial value.[138] Hahn echo decay is typically used to study the spin−spin relaxation, quantifying T_2.[80] A 90° pulse inside magnetic field flips the magnetization to the x−y plane. Then, spins in different environments begin to dephase at different speeds due to the local magnetic field inhomogeneities. Next, a 180° pulsed is used to flip the spin dephasing direction to remove the inhomogeneous dephasing so as to detect the magnetization. The process is repeated with different periods (t) of dephasing before the echo.[84,138]

$$M_{xy}(t) = M_{xy}(0)\exp(-t/T_2) \quad (3)$$

where $M_{xy}(0)$ and $M_{xy}(t)$ are the transverse components of the magnetization vector at time = 0 and t, respectively, and T_2 is the spin−spin relaxation time.

T_2 reflects the coherence time of the two spin states and thus the effectiveness of qubits. Recently, metal complexes with a long T_2 have been actively investigated as qubit candidates.[80,85−91] Finding a compound with a long T_2 is challenging, as interactions of unpaired electron spins in a compound with the local environment causes the rapid collapse of the superposition state through decoherence. Effects such as nuclear spin diffusion coupling to nearby electrons, methyl rotation, and spin diffusion barrier are major obstacles when it comes to prolonging the T_2. Zadrozny and co-workers have quantified μs-length T_2 of various d^1 V(IV) compounds and compared the spin−spin relaxation times with those of other well-known qubits such as the nitrogen-vacancy (NV) center. For example, T_2 = ∼1 ms for $(Ph_4P\text{-}d_{20})_2[V(C_8S_8)_3]$ in CS_2 at 10 K, eclipsing the nitrogen-vacancy center in nonisotopically enriched diamond.[82]

Pulsed X-band EPR experiments of a powder sample of **Co-TODA** (with no magnetic dilution of the Co^{II} ions) were performed at 5(1) K to give T_1 and T_2 times. Figure 7-Left gives the echo inversion recovery graph, giving the T_1 value of 235(4) μs at 5 K. It is interesting to note that, for **Co-TODA**, T_1 = 235(4) μs at 5(1) K, the lowest temperature measured in the current work, is in the same order as the relaxation time τ = 130 μs at 3.0 K, the highest temperature probed by alternating current (AC) susceptibility studies.[30] Figure 7 (right) shows the Hahn echo decay graph with the T_2 value of 0.513(4) μs at 5(1) K. It should be noted that the **Co-TODA** sample used here for the pulsed X-band EPR studies is 100% Co. The relatively short T_2 value suggests the presence of inter-Co^{II} magnetic interactions in **Co-TODA** that may be reduced with the use of diamagnetic Zn^{II} dilution. The field swept echo graphs in Figures S14 and S15 show one feature at 3344(1) G or approximately 0.33 T. The feature suggested an EPR observable intra-Kramers transition from ϕ_1 to ϕ_2. Due to the excitation bandwidth limitations, a pulsed X-band EPR sequence can only excite a portion of the spin populations. Moreover, not all spins can be flipped by a pulse at the same angle. Therefore, only one such transition can be observed in the spectra. T_1 and T_2 times at 10(1), 20(1), and 30(1) K were also measured. The echo inversion recovery and the Hahn echo decay graphs of the temperatures as well as the field swept echo graphs are given in the Supporting Information.

https://doi.org/10.1021/acs.jpcc.2c03083
J. Phys. Chem. C 2022, 126, 13268−13283

The T_2 time for **Co-TODA** is fairly long considering that there is no magnetic dilution in the CP and that the shortest $Co^{II}\cdots Co^{II}$ distance is 7.52 Å in the CP, making Zn^{II}-diluted **Co-TODA** potential qubit candidates. The rigid and sturdy structure of a CP and its unique phonon properties may provide an environment for the qubit centers in the CP, potentially prolonging T_2 times. Previous studies of the spin coherence times of qubit candidates were reported for Cu^{II}, Co^{II}, and V^{IV} CPs.[140−143] Yu, Freedman, and co-workers have shown that a magnetically diluted Cu^{II} porphyrin MOF at the 10, 40, and 100% levels has the phase memory time (T_m) values of 0.645, 0.121, and 0.046 μs, respectively.[142] T_m is the measure of all processes contributing to spin decoherence, including T_2. In the nondiluted CP, the distance between two nearest Cu^{II} centers is 13.595 Å. T_2 of 0.467 μs for **Co-TODA** is thus comparable to T_m of the 100% Cu^{II} porphyrin MOF, showing that **Co-TODA** is a promising qubit candidate. Another notable example is a Co^{II} porphyrin-based MOF investigated by Zadrozny, Freedman, and co-workers.[141] In the nonmagnetically diluted MOF, the distance between the two nearest Co^{II} neighbors is 13.643 Å. Once magnetically diluted to 7% of Co^{II} (with 93% of Zn^{II}), the T_2 time was found to be 13.74(9) μs.[141] The T_2 time is considerably longer than that of **Co-TODA** that is likely a result of the dilution of the Co^{II} magnetic centers as well as longer distances between the nearest Co^{II} neighbor in the structure. Further studies with Zn^{II}-diluted **Co-TODA** are needed to see if the diluted CP has qubit properties.

CONCLUSIONS

The versatility and power of the spectroscopic techniques in the characterization of molecular magnetism, especially the determination of the SH parameters, are highlighted in the current studies of powder samples of **Co-TODA** with field-induced slow magnetic relaxation. From physical chemistry perspectives, the current work demonstrates the power of advanced optical (FIRMS, HFEPR, pulsed EPR) and neutron (INS) spectroscopies in probing the magnetic properties of a metal-containing network. Results from the spectroscopies, combined with single-crystal X-ray diffraction at 15(2) K and ab initio calculations, offer a rare opportunity to understand the structure and properties of the CP in detail. FIRMS has revealed the inter-KD magnetic transition, and, together with HFEPR, led to a direct determination of the SH parameters (D, E, and g). In other words, the combined use of FIRMS and HFEPR is critical here for the deconvolution of the D' into the D and E values. Due to the large value of the E parameter, **Co-TODA** exhibits significant mixing of states, as demonstrated in the simulations of the FIRMS and HFEPR spectra. The electronic structure calculations in the current work have pointed out the origin of the magnetic anisotropy and the magnetostructural correlations, giving calculated SH parameters. The calculated SH parameters as well as the calculated DC susceptibility data are in support of the experimental findings, showcasing the utilities of the ab initio calculations. INS studies have given calculated INS spectra, phonon properties, and spin densities in the CP. The current work has also showcased that pulsed EPR is a unique tool in obtaining the magnetic relaxation times T_1 and T_2 for the intra-KD transition $\phi_1 \rightarrow \phi_2$. The T_2 time for the **Co-TODA** was found to be fairly long, with no magnetic dilution, compared to T_2 times of other transition-metal MOFs. The evidence suggested **Co-TODA** to be a potential qubit candidate. The calculated spin densities on the Co^{II} ions in **Co-TODA** and other high-spin Co^{II} complexes reported earlier reveal that the larger the spin density on a Co^{II} ion, the larger the ZFS in the complex.

ASSOCIATED CONTENT

Supporting Information

The Supporting Information is available free of charge at https://pubs.acs.org/doi/10.1021/acs.jpcc.2c03083.

Additional results from the calculations using CASPT2/RASSI-SO with MOLCAS 8.4; tables of the crystal structure of **Co-TODA** at 15(2) K and a comparison of selected bond lengths and angles of the crystal structures at 15(2) and 123(2) K; additional pulsed X-band EPR results; calculated spin densities in **Co-TODA** (PDF)

AUTHOR INFORMATION

Corresponding Author

Zi-Ling Xue − *Department of Chemistry, University of Tennessee, Knoxville, Tennessee 37996, United States;* orcid.org/0000-0001-7401-9933; Email: xue@utk.edu

Authors

Pagnareach Tin − *Department of Chemistry, University of Tennessee, Knoxville, Tennessee 37996, United States*

Alexandria N. Bone − *Department of Chemistry, University of Tennessee, Knoxville, Tennessee 37996, United States;* orcid.org/0000-0002-9967-7729

Nhat N. Bui − *National High Magnetic Field Laboratory, Florida State University, Tallahassee, Florida 32310, United States*

Yi-Quan Zhang − *Jiangsu Key Laboratory for NSLSCS, School of Physical Science and Technology, Nanjing Normal University, Nanjing 210023, China;* orcid.org/0000-0003-1818-0612

Tieyan Chang − *ChemMatCARS, Center for Advanced Radiation Sources, University of Chicago, Argonne, Illinois 60439, United States*

Duncan H. Moseley − *Department of Chemistry, University of Tennessee, Knoxville, Tennessee 37996, United States*

Mykhaylo Ozerov − *National High Magnetic Field Laboratory, Florida State University, Tallahassee, Florida 32310, United States;* orcid.org/0000-0002-5470-1158

J. Krzystek − *National High Magnetic Field Laboratory, Florida State University, Tallahassee, Florida 32310, United States;* orcid.org/0000-0001-6088-1936

Yongqiang Cheng − *Neutron Scattering Division, Oak Ridge National Laboratory, Oak Ridge, Tennessee 37831, United States;* orcid.org/0000-0002-3263-4812

Luke L. Daemen − *Neutron Scattering Division, Oak Ridge National Laboratory, Oak Ridge, Tennessee 37831, United States*

Xiaoping Wang − *Neutron Scattering Division, Oak Ridge National Laboratory, Oak Ridge, Tennessee 37831, United States;* orcid.org/0000-0001-7143-8112

Likai Song − *National High Magnetic Field Laboratory, Florida State University, Tallahassee, Florida 32310, United States*

Yu-Sheng Chen − *ChemMatCARS, Center for Advanced Radiation Sources, University of Chicago, Argonne, Illinois 60439, United States*

Dong Shao − *State Key Laboratory of Coordination Chemistry, School of Chemistry and Chemical Engineering, Nanjing University, Nanjing 210023, China;* orcid.org/0000-0002-3253-2680

Xin-Yi Wang − *State Key Laboratory of Coordination Chemistry, School of Chemistry and Chemical Engineering, Nanjing University, Nanjing 210023, China;* orcid.org/0000-0002-9256-1862

Xue-Tai Chen − *State Key Laboratory of Coordination Chemistry, School of Chemistry and Chemical Engineering, Nanjing University, Nanjing 210023, China;* orcid.org/0000-0001-5518-5557

Complete contact information is available at: https://pubs.acs.org/10.1021/acs.jpcc.2c03083

Notes

The authors declare no competing financial interest.

■ ACKNOWLEDGMENTS

US National Science Foundation (CHE-1900296 and CHE-2055499 to Z.-L.X.), Natural Science Grant of China (no. 21973046 to Y.-Q.Z.), and a Shull Wollan Center Graduate Research Fellowship (to P.T.) are acknowledged for partial support of the research. Part of this work was performed at the National High Magnetic Field Laboratory, which is supported by NSF Cooperative Agreement No. DMR-1644779 and the State of Florida. Neutron scattering experiments were conducted at the VISION beamline at ORNL's Spallation Neutron Source, which is supported by the Scientific User Facilities Division, Office of Basic Energy Sciences (BES), U.S. Department of Energy (DOE), under Contract No. DE-AC0500OR22725 with UT Battelle, LLC. The computing resources were made available through the VirtuES and the ICEMAN projects, funded by Laboratory Directed Research and Development program and Compute and Data Environment for Science (CADES) at ORNL. NSF's ChemMatCARS Sector 15 is supported by the Divisions of Chemistry (CHE) and Materials Research (DMR), National Science Foundation, under Grant Number NSF/CHE-1834750. Use of the Advanced Photon Source, an Office of Science User Facility operated for the U.S. Department of Energy (DOE) Office of Science by Argonne National Laboratory, was supported by the U.S. DOE under Contract No. DE-AC02-06CH11357. The authors thank Adam T. Hand and Michael J. Jenkins for help with FIRMS experiments.

■ REFERENCES

(1) Gatteschi, D.; Sessoli, R. Quantum Tunneling of Magnetization and Related Phenomena in Molecular Materials. *Angew. Chem., Int. Ed.* **2003**, *42*, 268−297.

(2) Ardavan, A.; Rival, O.; Morton, J. J. L.; Blundell, S. J.; Tyryshkin, A. M.; Timco, G. A.; Winpenny, R. E. P. Will Spin-Relaxation Times in Molecular Magnets Permit Quantum Information Processing? *Phys. Rev. Lett.* **2007**, *98*, No. 057201.

(3) Winpenny, R. E. P. Quantum information processing using molecular nanomagnets as qubits. *Angew. Chem., Int. Ed.* **2008**, *47*, 7992−7994.

(4) Rinehart, J. D.; Long, J. R. Exploiting single-ion anisotropy in the design of f-element single-molecule magnets. *Chem. Sci.* **2011**, *2*, 2078−2085.

(5) Gao, S. *Molecular Nanomagnets and Related Phenomena*; Springer: Berlin, 2015. https://link.springer.com/book/10.1007/978-3-662-45723-8.

(6) McInnes, E. J. L.; Winpenny, R. E. P. Molecular Magnets. In *Comprehensive Inorganic Chemistry II (Section 4.14)*; Reedijk, J.; Poeppelmeier, K., Eds.; Elsevier: Amsterdam, 2013; pp 371−395.

(7) Benelli, C.; Gatteschi, D. *Introduction to Molecular Magnetism: From Transition Metals to Lanthanides*; Wiley-VCH: New York, 2015. https://www.wiley.com/en-us/Introduction+to+Molecular+Magnetism%3A+From+Transition+Metals+to+Lanthanides-p-9783527335404.

(8) Frost, J. M.; Harriman, K. L. M.; Murugesu, M. The rise of 3-d single-ion magnets in molecular magnetism: towards materials from molecules? *Chem. Sci.* **2016**, *7*, 2470−2491.

(9) Lu, J.; Guo, M.; Tang, J. Recent Developments in Lanthanide Single-Molecule Magnets. *Chem.—Asian J.* **2017**, *12*, 2772−2779.

(10) Feng, M.; Tong, M.-L. Single Ion Magnets from 3d to 5f: Developments and Strategies. *Chem.—Eur. J.* **2018**, *24*, 7574−7594.

(11) Nain, S.; Khurana, R.; Ali, M. E. Harnessing Colossal Magnetic Anisotropy in Sandwiched $3d^2$-Metallocenes. *J. Phys. Chem. A* **2022**, *126*, 2811−2817.

(12) Berkley, R. S.; Hooshmand, Z.; Jiang, T.; Le, D.; Hebard, A. F.; Rahman, T. S. Characteristics of Single-Molecule Magnet Dimers ($[Mn_3]_2$) on Graphene and *h*-BN. *J. Phys. Chem. C* **2020**, *124*, 28186−28200.

(13) Tupolova, Y. P.; Shcherbakov, I. N.; Korchagin, D. V.; Tkachev, V. V.; Lebedev, V. E.; Popov, L. D.; Zakharov, K. V.; Vasiliev, A. N.; Palii, A. V.; Aldoshin, S. M. Fine-Tuning of Uniaxial Anisotropy and Slow Relaxation of Magnetization in the Hexacoordinate Co(II) Complexes with Acidoligands. *J. Phys. Chem. C* **2020**, *124*, 25957−25966.

(14) Yu, J.-X.; Christou, G.; Cheng, H.-P. Analysis of Exchange Interactions in Dimers of Mn_3 Single-Molecule Magnets, and Their Sensitivity to External Pressure. *J. Phys. Chem. C* **2020**, *124*, 14768−14774.

(15) Najafi, K.; Wysocki, A. L.; Park, K.; Economou, S. E.; Barnes, E. Toward Long-Range Entanglement between Electrically Driven Single-Molecule Magnets. *J. Phys. Chem. Lett.* **2019**, *10*, 7347−7355.

(16) Zabala-Lekuona, A.; Seco, J. M.; Colacio, E. Single-Molecule Magnets: From Mn_{12}-ac to dysprosium metallocenes, a travel in time. *Coord. Chem. Rev.* **2021**, *441*, No. 213984.

(17) Sarkar, A.; Dey, S.; Rajaraman, G. Role of Coordination Number and Geometry in Controlling the Magnetic Anisotropy in Fe^{II}, Co^{II}, and Ni^{II} Single-Ion Magnets. *Chem.—Eur. J.* **2020**, *26*, 14036−14058.

(18) Mínguez Espallargas, G.; Coronado, E. Magnetic functionalities in MOFs: from the framework to the pore. *Chem. Soc. Rev.* **2018**, *47*, 533−557.

(19) Sergeenko, A. S.; Ovens, J. S.; Leznoff, D. B. Designing anisotropic cyanometallate coordination polymers with unidirectional thermal expansion (TE): 2D zero and 1D colossal positive TE. *Chem. Commun.* **2018**, *54*, 1599−1602.

(20) Li, F.; Zhang, W.; Carné-Sánchez, A.; Tsujimoto, Y.; Kitagawa, S.; Furukawa, S.; Hu, M. Fighting at the Interface: Structural Evolution during Heteroepitaxial Growth of Cyanometallate Coordination Polymers. *Inorg. Chem.* **2018**, *57*, 8701−8704.

(21) Zhou, Y.; Abazari, R.; Chen, J.; Tahir, M.; Kumar, A.; Ikreedeegh, R. R.; Rani, E.; Singh, H.; Kirillov, A. M. Bimetallic metal−organic frameworks and MOF-derived composites: Recent progress on electro- and photoelectrocatalytic applications. *Coord. Chem. Rev.* **2022**, *451*, No. 214264.

(22) Dey, M.; Gogoi, N. Geometry-Mediated Enhancement of Single-Ion Anisotropy: A Route to Single-Molecule Magnets with a High Blocking Temperature. *Angew. Chem., Int. Ed.* **2013**, *52*, 12780−12782.

(23) Gómez-Coca, S.; Aravena, D.; Morales, R.; Ruiz, E. Large magnetic anisotropy in mononuclear metal complexes. *Coord. Chem. Rev.* **2015**, *289−290*, 379−392.

(24) Boča, R. Zero-field splitting in metal complexes. *Coord. Chem. Rev.* **2004**, *248*, 757−815.

(25) Aromí, G.; Brechin, E. K. Synthesis of 3d Metallic Single-Molecule Magnets. In *Single-Molecule Magnets and Related Phenomena*,

Winpenny, R., Ed.; Structure and Bonding; Springer, 2006; Vol. *122*, pp 1−67.
(26) Langley, S. K.; Wielechowski, D. P.; Vieru, V.; Chilton, N. F.; Moubaraki, B.; Abrahams, B. F.; Chibotaru, L. F.; Murray, K. S. A $\{Cr(III)_2Dy(III)_2\}$ Single-Molecule Magnet: Enhancing the Blocking Temperature through 3d Magnetic Exchange. *Angew. Chem., Int. Ed.* **2013**, *52*, 12014−12019.
(27) Krzystek, J.; Telser, J. Measuring giant anisotropy in paramagnetic transition metal complexes with relevance to single-ion magnetism. *Dalton Trans.* **2016**, *45*, 16751−16763.
(28) Moseley, D. H.; Stavretis, S. E.; Thirunavukkuarasu, K.; Ozerov, M.; Cheng, Y.; Daemen, L. L.; Ludwig, J.; Lu, Z.; Smirnov, D.; Brown, C. M.; et al. Spin-phonon couplings in transition metal complexes with slow magnetic relaxation. *Nat. Commun.* **2018**, *9*, No. 2572.
(29) Krzystek, J.; Zvyagin, S. A.; Ozarowski, A.; Fiedler, A. T.; Brunold, T. C.; Telser, J. Definitive Spectroscopic Determination of Zero-Field Splitting in High-Spin Cobalt(II). *J. Am. Chem. Soc.* **2004**, *126*, 2148−2155.
(30) Shao, D.; Zhou, Y.; Pi, Q.; Shen, F.-X.; Yang, S.-R.; Zhang, S.-L.; Wang, X.-Y. Two-dimensional frameworks formed by pentagonal bipyramidal cobalt(II) ions and hexacyanometallates: antiferromagnetic ordering, metamagnetism and slow magnetic relaxation. *Dalton Trans.* **2017**, *46*, 9088−9096.
(31) McGavin, D. G. Symmetry constraints on EPR spin-Hamiltonian parameters. *J. Magn. Reson. (1969)* **1987**, *74*, 19−55.
(32) Pilbrow, J. R. Effective g values for $S = 3/2$ and $S = 5/2$. *J. Magn. Reson. (1969)* **1978**, *31*, 479−490.
(33) Gast, P.; Groenen, E. J. J. EPR Interactions − g-Anisotropy. *eMagRes* **2007**, 1435−1444.
(34) Zadrozny, J. M.; Liu, J.; Piro, N. A.; Chang, C. J.; Hill, S.; Long, J. R. Slow magnetic relaxation in a pseudotetrahedral cobalt(II) complex with easy-plane anisotropy. *Chem. Commun.* **2012**, *48*, 3927−3929.
(35) Vallejo, J.; Castro, I.; Ruiz-García, R.; Cano, J.; Julve, M.; Lloret, F.; De Munno, G.; Wernsdorfer, W.; Pardo, E. Field-Induced Slow Magnetic Relaxation in a Six-Coordinate Mononuclear Cobalt(II) Complex with a Positive Anisotropy. *J. Am. Chem. Soc.* **2012**, *134*, 15704−15707.
(36) Colacio, E.; Ruiz, J.; Ruiz, E.; Cremades, E.; Krzystek, J.; Carretta, S.; Cano, J.; Guidi, T.; Wernsdorfer, W.; Brechin, E. K. Slow Magnetic Relaxation in a Co^{II}−Y^{III} Single-Ion Magnet with Positive Axial Zero-Field Splitting. *Angew. Chem., Int. Ed.* **2013**, *52*, 9130−9134.
(37) Huang, W.; Liu, T.; Wu, D.; Cheng, J.; Ouyang, Z. W.; Duan, C. Field-induced slow relaxation of magnetization in a tetrahedral Co(II) complex with easy plane anisotropy. *Dalton Trans.* **2013**, *42*, 15326−15331.
(38) Wu, D.; Zhang, X.; Huang, P.; Huang, W.; Ruan, M.; Ouyang, Z. W. Tuning Transverse Anisotropy in Co^{III}−Co^{II}−Co^{III} Mixed-Valence Complex toward Slow Magnetic Relaxation. *Inorg. Chem.* **2013**, *52*, 10976−10982.
(39) Zadrozny, J. M.; Atanasov, M.; Bryan, A. M.; Lin, C.-Y.; Rekken, B. D.; Power, P. P.; Neese, F.; Long, J. R. Slow magnetization dynamics in a series of two-coordinate iron(II) complexes. *Chem. Sci.* **2013**, *4*, 125−138.
(40) Wang, J.; Cui, H.-H.; Zhang, Y.-Q.; Chen, L.; Chen, X.-T. Magnetic anisotropy and slow magnetic relaxation of seven-coordinate cobalt(II)−nitrate complexes. *Polyhedron* **2018**, *154*, 148−155.
(41) Cui, H.-H.; Zhang, Y.-Q.; Chen, X.-T.; Wang, Z.; Xue, Z.-L. Magnetic anisotropy and slow magnetic relaxation processes of cobalt(II)-pseudohalide complexes. *Dalton Trans.* **2019**, *48*, 10743−10752.
(42) Cui, H.-H.; Ding, M.-M.; Zhang, X.-D.; Lv, W.; Zhang, Y.-Q.; Chen, X.-T.; Wang, Z.; Ouyang, Z.-W.; Xue, Z.-L. Magnetic anisotropy in square pyramidal cobalt(II) complexes supported by a tetraazo macrocyclic ligand. *Dalton Trans.* **2020**, *49*, 14837−14846.
(43) Chen, L.; Chen, S.-Y.; Sun, Y.-C.; Guo, Y.-M.; Yu, L.; Chen, X.-T.; Wang, Z.; Ouyang, Z. W.; Song, Y.; Xue, Z.-L. Slow magnetic relaxation in mononuclear seven-coordinate cobalt(II) complexes with easy plane anisotropy. *Dalton Trans.* **2015**, *44*, 11482−11490.
(44) Samuel, P. P.; Mondal, K. C.; Amin Sk, N.; Roesky, H. W.; Carl, E.; Neufeld, R.; Stalke, D.; Demeshko, S.; Meyer, F.; Ungur, L.; et al. Electronic Structure and Slow Magnetic Relaxation of Low-Coordinate Cyclic Alkyl(amino) Carbene Stabilized Iron(I) Complexes. *J. Am. Chem. Soc.* **2014**, *136*, 11964−11971.
(45) Lv, W.; Cui, H.-H.; Chen, L.; Zhang, Y.-Q.; Chen, X.-t.; Wang, Z.; Ouyang, Z.; Xue, Z.-L. Magnetic anisotropy of two tetrahedral Co(II)-halide complexes with triphenylphosphine ligands. *Dalton Trans.* **2022**, *51*, 7530−7538.
(46) Telser, J.; Ozarowski, A.; Krzystek, J. High-frequency and -field electron paramagnetic resonance of transition metal ion (d block) coordination complexes. *Electron Paramagn. Reson.* **2012**, *23*, 209−263.
(47) Solomon, E. I.; Pavel, E. G.; Loeb, K. E.; Campochiaro, C. Magnetic circular dichroism spectroscopy as a probe of the geometric and electronic structure of non-heme ferrous enzymes. *Coord. Chem. Rev.* **1995**, *144*, 369−460.
(48) Bone, A. N.; Widener, C. N.; Moseley, D. H.; Liu, Z.; Lu, Z.; Cheng, Y.; Daemen, L. L.; Ozerov, M.; Telser, J.; Thirunavukkuarasu, K.; et al. Applying Unconventional Spectroscopies to the Single-Molecule Magnets, $Co(PPh_3)_2X_2$ (X = Cl, Br, I): Unveiling Magnetic Transitions and Spin-Phonon Coupling. *Chem.—Eur. J.* **2021**, *27*, 11110−11125.
(49) Brackett, G. C.; Richards, P. L.; Caughey, W. S. Far-Infrared Magnetic Resonance in Fe(III) and Mn(III) Porphyrins, Myoglobin, Hemoglobin, Ferrichrome A, and Fe(III) Dithiocarbamates. *J. Chem. Phys.* **1971**, *54*, 4383−4401.
(50) Uenoyama, H. Far-infrared studies on hemin and hemin-like complexes. *Biochim. Biophys. Acta, Gen. Subj.* **1971**, *230*, 479−481.
(51) Jiang, S.-D.; Maganas, D.; Levesanos, N.; Ferentinos, E.; Haas, S.; Thirunavukkuarasu, K.; Krzystek, J.; Dressel, M.; Bogani, L.; Neese, F.; Kyritsis, P. Direct Observation of Very Large Zero-Field Splitting in a Tetrahedral $Ni^{II}Se_4$ Coordination Complex. *J. Am. Chem. Soc.* **2015**, *137*, 12923−12928.
(52) Slota, M.; Jiang, S.-D.; Heintze, E.; Rechkemmer, Y.; Dressel, M.; van Slageren, J.; Bogani, L. Accurate and unequivocal determination of the crystal-field parameters of lanthanide ions via a multitechnique approach. *Phys. Rev. B* **2019**, *99*, No. 134410.
(53) Stavretis, S. E.; Moseley, D. H.; Fei, F.; Cui, H.-H.; Cheng, Y.; Podlesnyak, A. A.; Wang, X.; Daemen, L. L.; Hoffmann, C. M.; Ozerov, M.; et al. Spectroscopic Studies of the Magnetic Excitation and Spin-Phonon Couplings in a Single-Molecule Magnet. *Chem.—Eur. J.* **2019**, *25*, 15846−15857.
(54) Moseley, D. H.; Stavretis, S. E.; Zhu, Z.; Guo, M.; Brown, C. M.; Ozerov, M.; Cheng, Y.; Daemen, L. L.; Richardson, R.; Knight, G.; et al. Inter-Kramers Transitions and Spin-Phonon Couplings in a Lanthanide-Based Single-Molecule Magnet. *Inorg. Chem.* **2020**, *59*, 5218−5230.
(55) Tin, P.; Stavretis, S. E.; Ozerov, M.; Krzystek, J.; Ponomaryov, A. N.; Zvyagin, S. A.; Wosnitza, J.; Chen, C.-C.; Chen, P. P. Y.; Telser, J.; Xue, Z. L. Advanced Magnetic Resonance Studies of Tetraphenylporphyrinatoiron(III) Halides. *Appl. Magn. Reson.* **2020**, *51*, 1411−1432.
(56) Widener, C. N.; Bone, A. N.; Ozerov, M.; Richardson, R.; Lu, Z.; Thirunavukkuarasu, K.; Smirnov, D.; Chen, X.-T.; Xue, Z.-L. Direct Observation of Magnetic Transitions in a Nickel(II) Complex with Large Anisotropy. *Chin. J. Inorg. Chem.* **2020**, *36*, 1149−1156.
(57) Blockmon, A. L.; Ullah, A.; Hughey, K. D.; Duan, Y.; O'Neal, K. R.; Ozerov, M.; Baldoví, J. J.; Aragó, J.; Gaita-Ariño, A.; Coronado, E.; Musfeldt, J. L. Spectroscopic Analysis of Vibronic Relaxation Pathways in Molecular Spin Qubit $[Ho(W_5O_{18})_2]^{9-}$: Sparse Spectra Are Key. *Inorg. Chem.* **2021**, *60*, 14096−14104.
(58) Brackett, G. C. Far-Infrared Magnetic Resonance in Fe(III) and Mn(III) Porphyrins, Myoglobin, Hemoglobin, Ferrichrome A, and Fe(III) Dithiocarbamates. Ph.D. Dissertation, University of California: Berkeley, 1970. https://www.osti.gov/servlets/purl/4081228.

https://doi.org/10.1021/acs.jpcc.2c03083
J. Phys. Chem. C 2022, 126, 13268−13283

(59) Liu, J.-J.; Meng, Y.-S.; Hlavicka, I.; Orlita, M.; Jiang, S.-D.; Wang, B.-W.; Gao, S. Determination of zero-field splitting in Co^{2+} halide complexes with magnetic and far-IR measurements. *Dalton Trans.* **2017**, *46*, 7408−7411.
(60) Schnegg, A.; Behrends, J.; Lips, K.; Bittl, R.; Holldack, K. Frequency domain Fourier transform THz-EPR on single molecule magnets using coherent synchrotron radiation. *Phys. Chem. Chem. Phys.* **2009**, *11*, 6820−6825.
(61) Lu, J.; Ozel, I. O.; Belvin, C. A.; Li, X.; Skorupskii, G.; Sun, L.; Ofori-Okai, B. K.; Dincă, M.; Gedik, N.; Nelson, K. A. Rapid and precise determination of zero-field splittings by terahertz time-domain electron paramagnetic resonance spectroscopy. *Chem. Sci.* **2017**, *8*, 7312−7323.
(62) Bloor, D.; Copland, G. M. Far infrared spectra of magnetic ions in crystals. *Rep. Progr. Phys.* **1972**, *35*, 1173−1264.
(63) Vallejo, J.; Viciano-Chumillas, M.; Lloret, F.; Julve, M.; Castro, I.; Krzystek, J.; Ozerov, M.; Armentano, D.; De Munno, G.; Cano, J. Coligand Effects on the Field-Induced Double Slow Magnetic Relaxation in Six-Coordinate Cobalt(II) Single-Ion Magnets (SIMs) with Positive Magnetic Anisotropy. *Inorg. Chem.* **2019**, *58*, 15726−15740.
(64) Kumar, P.; SantaLucia, D. J.; Kaniewska-Laskowska, K.; Lindeman, S. V.; Ozarowski, A.; Krzystek, J.; Ozerov, M.; Telser, J.; Berry, J. F.; Fiedler, A. T. Probing the Magnetic Anisotropy of Co(II) Complexes Featuring Redox-Active Ligands. *Inorg. Chem.* **2020**, *59*, 16178−16193.
(65) Landart-Gereka, A.; Quesada-Moreno, M. M.; Díaz-Ortega, I. F.; Nojiri, H.; Ozerov, M.; Krzystek, J.; Palacios, M. A.; Colacio, E. Large easy-axis magnetic anisotropy in a series of trigonal prismatic mononuclear cobalt(II) complexes with zero-field hidden single-molecule magnet behaviour: the important role of the distortion of the coordination sphere and intermolecular interactions in the slow relaxation. *Inorg. Chem. Front.* **2022**, *9*, 2810−2831.
(66) Bacon, G. E. *Neutron Scattering in Chemistry*; Butterworth: London, 1977.
(67) Basler, R.; Boskovic, C.; Chaboussant, G.; Güdel, H. U.; Murrie, M.; Ochsenbein, S. T.; Sieber, A. Molecular Spin Clusters: New Synthetic Approaches and Neutron Scattering Studies. *ChemPhysChem* **2003**, *4*, 910−926.
(68) Giansiracusa, M. J.; Vonci, M.; Van den Heuvel, W.; Gable, R. W.; Moubaraki, B.; Murray, K. S.; Yu, D.; Mole, R. A.; Soncini, A.; Boskovic, C. Carbonate-Bridged Lanthanoid Triangles: Single-Molecule Magnet Behavior, Inelastic Neutron Scattering, and Ab Initio Studies. *Inorg. Chem.* **2016**, *55*, 5201−5214.
(69) Dunstan, M. A.; Mole, R. A.; Boskovic, C. Inelastic Neutron Scattering of Lanthanoid Complexes and Single-Molecule Magnets. *Eur. J. Inorg. Chem.* **2019**, *2019*, 1090−1105.
(70) Chen, L.; Cui, H.-H.; Stavretis, S. E.; Hunter, S. C.; Zhang, Y.-Q.; Chen, X.-T.; Sun, Y.-C.; Wang, Z.; Song, Y.; Podlesnyak, A. A.; Ouyang, Z.-W.; Xue, Z. L. Slow Magnetic Relaxations in Cobalt(II) Tetranitrate Complexes. Studies of Magnetic Anisotropy by Inelastic Neutron Scattering and High-Frequency and High-Field EPR Spectroscopy. *Inorg. Chem.* **2016**, *55*, 12603−12617.
(71) Bone, A. N.; Stavretis, S. E.; Krzystek, J.; Liu, Z.; Chen, Q.; Gai, Z.; Wang, X.; Steren, C. A.; Powers, X. B.; Podlesnyak, A. A.; et al. Manganese tetraphenylporphyrin bromide and iodide. Studies of structures and magnetic properties. *Polyhedron* **2020**, *184*, No. 114488.
(72) Xue, Z.-L.; Ramirez-Cuesta, A. J.; Brown, C. M.; Calder, S.; Cao, H.; Chakoumakos, B. C.; Daemen, L. L.; Huq, A.; Kolesnikov, A. I.; Mamontov, E.; et al. Neutron Instruments for Research in Coordination Chemistry. *Eur. J. Inorg. Chem.* **2019**, *2019*, 1065−1089.
(73) Stavretis, S. E.; Cheng, Y.; Daemen, L. L.; Brown, C. M.; Moseley, D. H.; Bill, E.; Atanasov, M.; Ramirez-Cuesta, A. J.; Neese, F.; Xue, Z.-L. Probing Magnetic Excitations in CoII Single-Molecule Magnets by Inelastic Neutron Scattering. *Eur. J. Inorg. Chem.* **2019**, *2019*, 1119−1127.
(74) VASP, The Vienna Ab initio Simulation Package: Atomic Scale Materials Modelling from First Principles. http://hdl.handle.net/11256/491.
(75) Togo, A. VASP & Phonopy Calculation, 2009. https://phonopy.github.io/phonopy/vasp-dfpt.html.
(76) Cheng, Y. Q.; Daemen, L. L.; Kolesnikov, A. I.; Ramirez-Cuesta, A. J. Simulation of Inelastic Neutron Scattering Spectra Using OCLIMAX. *J. Chem. Theory Comput.* **2019**, *15*, 1974−1982.
(77) Stavretis, S. E.; Mamontov, E.; Moseley, D. H.; Cheng, Y.; Daemen, L. L.; Ramirez-Cuesta, A. J.; Xue, Z.-L. Effect of magnetic fields on the methyl rotation in a paramagnetic cobalt(II) complex. Quasielastic neutron scattering studies. *Phys. Chem. Chem. Phys.* **2018**, *20*, 21119−21126.
(78) Mills, D. P.; Moro, F.; McMaster, J.; van Slageren, J.; Lewis, W.; Blake, A. J.; Liddle, S. T. A delocalized arene-bridged diuranium single-molecule magnet. *Nat. Chem.* **2011**, *3*, 454−460.
(79) Wang, Z.; Datta, S.; Papatriantafyllopoulou, C.; Christou, G.; Dalal, N. S.; van Tol, J.; Hill, S. Spin decoherence in an iron-based magnetic cluster. *Polyhedron* **2011**, *30*, 3193−3196.
(80) Aravena, D.; Ruiz, E. Spin dynamics in single-molecule magnets and molecular qubits. *Dalton Trans.* **2020**, *49*, 9916−9928.
(81) Abeywardana, C.; Mowson, A. M.; Christou, G.; Takahashi, S. Spin coherence in a Mn_3 single-molecule magnet. *Appl. Phys. Lett.* **2016**, *108*, No. 042401.
(82) Zadrozny, J. M.; Niklas, J.; Poluektov, O. G.; Freedman, D. E. Millisecond Coherence Time in a Tunable Molecular Electronic Spin Qubit. *ACS Cent. Sci.* **2015**, *1*, 488−492.
(83) Hill, S.; Edwards, R. S.; Aliaga-Alcalde, N.; Christou, G. Quantum Coherence in an Exchange-Coupled Dimer of Single-Molecule Magnets. *Science* **2003**, *302*, 1015−1018.
(84) Webber, R. T. *Pulsed EPR Primer*; Bruker Instruments, Inc., 2000.
(85) Graham, M. J.; Zadrozny, J. M.; Fataftah, M. S.; Freedman, D. E. Forging Solid-State Qubit Design Principles in a Molecular Furnace. *Chem. Mater.* **2017**, *29*, 1885−1897.
(86) Gaita-Ariño, A.; Prima-Garcia, H.; Cardona-Serra, S.; Escalera-Moreno, L.; Rosaleny, L. E.; Baldovi, J. J. Coherence and organisation in lanthanoid complexes: from single ion magnets to spin qubits. *Inorg. Chem. Front.* **2016**, *3*, 568−577.
(87) Ding, Y.-S.; Deng, Y.-F.; Zheng, Y.-Z. The rise of single-ion magnets as spin qubits. *Magnetochemistry* **2016**, *2*, No. 40.
(88) von Kugelgen, S.; Freedman, D. E. A chemical path to quantum information. *Science* **2019**, *366*, 1070−1071.
(89) Aromí, G.; Aguilà, D.; Gamez, P.; Luis, F.; Roubeau, O. Design of magnetic coordination complexes for quantum computing. *Chem. Soc. Rev.* **2012**, *41*, 537−546.
(90) Bader, K.; Schlindwein, S. H.; Gudat, D.; van Slageren, J. Molecular qubits based on potentially nuclear-spin-free nickel ions. *Phys. Chem. Chem. Phys.* **2017**, *19*, 2525−2529.
(91) Atzori, M.; Morra, E.; Tesi, L.; Albino, A.; Chiesa, M.; Sorace, L.; Sessoli, R. Quantum Coherence Times Enhancement in Vanadium(IV)-based Potential Molecular Qubits: the Key Role of the Vanadyl Moiety. *J. Am. Chem. Soc.* **2016**, *138*, 11234−11244.
(92) Muñoz, M. C.; Real, J. A. Thermo-, piezo-, photo- and chemo-switchable spin crossover iron(II)-metallocyanate based coordination polymers. *Coord. Chem. Rev.* **2011**, *255*, 2068−2093.
(93) Train, C.; Gruselle, M.; Verdaguer, M. The fruitful introduction of chirality and control of absolute configurations in molecular magnets. *Chem. Soc. Rev.* **2011**, *40*, 3297−3312.
(94) Pinkowicz, D.; Southerland, H. I.; Avendaño, C.; Prosvirin, A.; Sanders, C.; Wernsdorfer, W.; Pedersen, K. S.; Dreiser, J.; Clérac, R.; Nehrkorn, J.; et al. Cyanide Single-Molecule Magnets Exhibiting Solvent Dependent Reversible "On" and "Off" Exchange Bias Behavior. *J. Am. Chem. Soc.* **2015**, *137*, 14406−14422.
(95) Pinkowicz, D.; Southerland, H.; Wang, X.-Y.; Dunbar, K. R. Record Antiferromagnetic Coupling for a 3d/4d Cyanide-Bridged Compound. *J. Am. Chem. Soc.* **2014**, *136*, 9922−9924.
(96) Wei, R.-M.; Cao, F.; Li, J.; Yang, L.; Han, Y.; Zhang, X.-L.; Zhang, Z.; Wang, X.-Y.; Song, Y. Single-Chain Magnets Based on

Octacyanotungstate with the Highest Energy Barriers for Cyanide Compounds. *Sci. Rep.* **2016**, *6*, No. 24372.
(97) Hassan, A. K.; Pardi, L. A.; Krzystek, J.; Sienkiewicz, A.; Goy, P.; Rohrer, M.; Brunel, L. C. Ultrawide Band Multifrequency High-Field EMR Technique: A Methodology for Increasing Spectroscopic Information. *J. Magn. Reson.* **2000**, *142*, 300−312.
(98) Seeger, P. A.; Daemen, L. L.; Larese, J. Z. Resolution of VISION, a crystal-analyzer spectrometer. *Nucl. Instrum. Methods Phys. Res., Sect. A* **2009**, *604*, 719−728.
(99) Mitchell, P. C. H.; Parker, S. F.; Ramirez-Cuesta, A. J.; Tomkinson, J. *Vibrational Spectroscopy with Neutrons: With Applications in Chemistry, Biology, Materials Science and Catalysis*, Series on Neutron Techniques and Applications; World Scientific Publishing Company, 2005. https://www.worldscientific.com/worldscibooks/10.1142/5628.
(100) Aquilante, F.; Autschbach, J.; Carlson, R. K.; Chibotaru, L. F.; Delcey, M. G.; De Vico, L.; Fdez; Galvan, I.; Ferre, N.; Frutos, L. M.; Gagliardi, L.; et al. Molcas 8: New capabilities for multiconfigurational quantum chemical calculations across the periodic table. *J. Comput. Chem.* **2016**, *37*, 506−541.
(101) Chibotaru, L. F.; Ungur, L.; Soncini, A. The origin of nonmagnetic Kramers doublets in the ground state of dysprosium triangles: evidence for a toroidal magnetic moment. *Angew. Chem., Int. Ed.* **2008**, *47*, 4126−4129.
(102) Ungur, L.; Van den Heuvel, W.; Chibotaru, L. F. Ab initio investigation of the non-collinear magnetic structure and the lowest magnetic excitations in dysprosium triangles. *New J. Chem.* **2009**, *33*, 1224−1230.
(103) Chibotaru, L. F.; Ungur, L.; Aronica, C.; Elmoll, H.; Pilet, G.; Luneau, D. Structure, Magnetism, and Theoretical Study of a Mixed-Valence $Co(II)_3Co(III)_4$ Heptanuclear Wheel: Lack of SMM Behavior despite Negative Magnetic Anisotropy. *J. Am. Chem. Soc.* **2008**, *130*, 12445−12455.
(104) Neese, F. *ORCA—An Ab Initio, Density Functional and Semiempirical Program Package*, version 4.2; Max-Planck Institute For Bioinorganic Chemistry: Mülheim an der Ruhr, Germany, 2019.
(105) Heß, B. A.; Marian, C. M.; Wahlgren, U.; Gropen, O. A mean-field spin-orbit method applicable to correlated wavefunctions. *Chem. Phys. Lett.* **1996**, *251*, 365−371.
(106) Angeli, C.; Cimiraglia, R.; Evangelisti, S.; Leininger, T.; Malrieu, J. P. Introduction of n-electron valence states for multi-reference perturbation theory. *J. Chem. Phys.* **2001**, *114*, 10252−10264.
(107) Angeli, C.; Cimiraglia, R.; Malrieu, J.-P. N-electron valence state perturbation theory: a fast implementation of the strongly contracted variant. *Chem. Phys. Lett.* **2001**, *350*, 297−305.
(108) Angeli, C.; Cimiraglia, R. Multireference perturbation configuration interaction V. Third-order energy contributions in the Moller-Plesset and Epstein-Nesbet partitions. *Theor. Chem. Acc.* **2002**, *107*, 313−317.
(109) Angeli, C.; Cimiraglia, R.; Malrieu, J.-P. n-Electron valence state perturbation theory: A spinless formulation and an efficient implementation of the strongly contracted and of the partially contracted variants. *J. Chem. Phys.* **2002**, *117*, 9138−9153.
(110) Schäfer, A.; Horn, H.; Ahlrichs, R. Fully optimized contracted Gaussian basis sets for atoms Li to Kr. *J. Chem. Phys.* **1992**, *97*, 2571−2577.
(111) Schäfer, A.; Huber, C.; Ahlrichs, R. Fully optimized contracted Gaussian basis sets of triple zeta valence quality for atoms Li to Kr. *J. Chem. Phys.* **1994**, *100*, 5829−5835.
(112) Weigend, F.; Ahlrichs, R. Balanced basis sets of split valence, triple zeta valence and quadruple zeta valence quality for H to Rn: Design and assessment of accuracy. *Phys. Chem. Chem. Phys.* **2005**, *7*, 3297−3305.
(113) Kresse, G.; Furthmueller, J. Efficient iterative schemes for ab initio total-energy calculations using a plane-wave basis set. *Phys. Rev. B* **1996**, *54*, 11169−11186.
(114) Blöchl, P. E. Projector augmented-wave method. *Phys. Rev. B* **1994**, *50*, 17953−17979.
(115) Kresse, G.; Joubert, D. From ultrasoft pseudopotentials to the projector augmented-wave method. *Phys. Rev. B* **1999**, *59*, 1758−1775.
(116) Perdew, J. P.; Burke, K.; Ernzerhof, M. Generalized gradient approximation made simple. *Phys. Rev. Lett.* **1996**, *77*, 3865−3868.
(117) Klimeš, J.; Bowler, D. R.; Michaelides, A. Chemical accuracy for the van der Waals density functional. *J. Phys.: Condens. Matter* **2010**, *22*, No. 022201.
(118) Wang, L.; Maxisch, T.; Ceder, G. Oxidation energies of transition metal oxides within the GGA+*U* framework. *Phys. Rev. B* **2006**, *73*, No. 195107.
(119) Togo, A.; Tanaka, I. First principles phonon calculations in materials science. *Scr. Mater.* **2015**, *108*, 1−5.
(120) Stoll, S.; Schweiger, A. EasySpin, a comprehensive software package for spectral simulation and analysis in EPR. *J. Magn. Reson.* **2006**, *178*, 42−55.
(121) Ryder, M. R.; Van de Voorde, B.; Civalleri, B.; Bennett, T. D.; Mukhopadhyay, S.; Cinque, G.; Fernandez-Alonso, F.; De Vos, D.; Rudić, S.; Tan, J.-C. Detecting Molecular Rotational Dynamics Complementing the Low-Frequency Terahertz Vibrations in a Zirconium-Based Metal-Organic Framework. *Phys. Rev. Lett.* **2017**, *118*, No. 255502.
(122) Escalera-Moreno, L.; Baldoví, J. J.; Gaita-Ariño, A.; Coronado, E. Spin states, vibrations and spin relaxation in molecular nanomagnets and spin qubits: A critical perspective. *Chem. Sci.* **2018**, *9*, 3265−3275.
(123) Lunghi, A.; Totti, F.; Sanvito, S.; Sessoli, R. Intra-molecular origin of the spin-phonon coupling in slow-relaxing molecular magnets. *Chem. Sci.* **2017**, *8*, 6051−6059.
(124) Lunghi, A.; Sanvito, S. How do phonons relax molecular spins? *Sci. Adv.* **2019**, *5*, No. eaax7163.
(125) Mirzoyan, R.; Hadt, R. G. The dynamic ligand field of a molecular qubit: decoherence through spin−phonon coupling. *Phys. Chem. Chem. Phys.* **2020**, *22*, 11249−11265.
(126) Gómez-Coca, S.; Urtizberea, A.; Cremades, E.; Alonso, P. J.; Camón, A.; Ruiz, E.; Luis, F. Origin of slow magnetic relaxation in Kramers ions with non-uniaxial anisotropy. *Nat. Commun.* **2014**, *5*, No. 4300.
(127) Sherwood, P. M. A. *Vibrational Spectroscopy of Solids*; Cambridge University Press, 1972; p 254. https://www.cambridge.org/us/academic/subjects/chemistry/chemistry-general-interest/vibrational-spectroscopy-solids?format=HB&isbn=9780521279147.
(128) Hunter, S. C.; Podlesnyak, A. A.; Xue, Z.-L. Magnetic Excitations in Metalloporphyrins by Inelastic Neutron Scattering: Determination of Zero-Field Splittings in Iron, Manganese, and Chromium Complexes. *Inorg. Chem.* **2014**, *53*, 1955−1961.
(129) Atanasov, M.; Ganyushin, D.; Sivalingam, K.; Neese, F. A Modern First-Principles View on Ligand Field Theory Through the Eyes of Correlated Multireference Wavefunctions. In *Molecular Electronic Structures of Transition Metal Complexes II*; Mingos, D. M. P.; Day, P.; Dahl, J. P., Eds.; Springer: Heidelberg, 2012; pp 149−220. https://link.springer.com/chapter/10.1007/430_2011_57.
(130) Singh, S. K.; Eng, J.; Atanasov, M.; Neese, F. Covalency and chemical bonding in transition metal complexes: An ab initio based ligand field perspective. *Coord. Chem. Rev.* **2017**, *344*, 2−25.
(131) Gomez-Coca, S.; Cremades, E.; Aliaga-Alcalde, N.; Ruiz, E. Mononuclear Single-Molecule Magnets: Tailoring the Magnetic Anisotropy of First-Row Transition-Metal Complexes. *J. Am. Chem. Soc.* **2013**, *135*, 7010−7018.
(132) Craven, M.; Nygaard, M. H.; Zadrozny, J. M.; Long, J. R.; Overgaard, J. Determination of d-Orbital Populations in a Cobalt(II) Single-Molecule Magnet Using Single-Crystal X-ray Diffraction. *Inorg. Chem.* **2018**, *57*, 6913−6920.
(133) Bunting, P. C.; Atanasov, M.; Damgaard-Moller, E.; Perfetti, M.; Crassee, I.; Orlita, M.; Overgaard, J.; van Slageren, J.; Neese, F.; Long, J. R. A linear cobalt(II) complex with maximal orbital angular momentum from a non-Aufbau ground state. *Science* **2018**, *362*, No. eaat7319.

(134) Zhou, F.; Cococcioni, M.; Marianetti, C. A.; Morgan, D.; Ceder, G. First-principles prediction of redox potentials in transition-metal compounds with LDA+U. *Phys. Rev. B* **2004**, *70*, No. 235121.
(135) Chen, J.; Wu, X.; Selloni, A. Electronic structure and bonding properties of cobalt oxide in the spinel structure. *Phys. Rev. B* **2011**, *83*, No. 245204.
(136) Schlegel, C.; van Slageren, J.; Manoli, M.; Brechin, E. K.; Dressel, M. Direct Observation of Quantum Coherence in Single-Molecule Magnets. *Phys. Rev. Lett.* **2008**, *101*, No. 147203.
(137) Fataftah, M. S.; Krzyaniak, M. D.; Vlaisavljevich, B.; Wasielewski, M. R.; Zadrozny, J. M.; Freedman, D. E. Metal-ligand covalency enables room temperature molecular qubit candidates. *Chem. Sci.* **2019**, *10*, 6707−6714.
(138) Bloch, F. Nuclear induction. *Phys. Rev.* **1946**, *70*, 460−474.
(139) Goldman, M. Formal theory of spin-lattice relaxation. *J. Magn. Reson.* **2001**, *149*, 160−187.
(140) Urtizberea, A.; Natividad, E.; Alonso, P. J.; Andres, M. A.; Gascon, I.; Goldmann, M.; Roubeau, O. A Porphyrin Spin Qubit and Its 2D Framework Nanosheets. *Adv. Funct. Mater.* **2018**, *28*, No. 1801695.
(141) Zadrozny, J. M.; Gallagher, A. T.; Harris, T. D.; Freedman, D. E. A Porous Array of Clock Qubits. *J. Am. Chem. Soc.* **2017**, *139*, 7089−7094.
(142) Yu, C.-J.; Krzyaniak, M. D.; Fataftah, M. S.; Wasielewski, M. R.; Freedman, D. E. A concentrated array of copper porphyrin candidate qubits. *Chem. Sci.* **2019**, *10*, 1702−1708.
(143) Yamabayashi, T.; Atzori, M.; Tesi, L.; Cosquer, G.; Santanni, F.; Boulon, M.-E.; Morra, E.; Benci, S.; Torre, R.; Chiesa, M.; et al. Scaling Up Electronic Spin Qubits into a Three-Dimensional Metal-Organic Framework. *J. Am. Chem. Soc.* **2018**, *140*, 12090−12101.

https://doi.org/10.1021/acs.jpcc.2c03083
J. Phys. Chem. C 2022, 126, 13268−13283